IEEE Open Journal of the
Industrial Electronics Society

Received 4 March 2024; revised 24 March 2024, 2 April 2024, and 3 April 2024; accepted 8 April 2024. Date of publication 11 April 2024; date of current version 24 April 2024. The review of this article was arranged by Associate Editor Xinbo Ruan.

Digital Object Identifier 10.1109/OJIES.2024.3387432

High-Current Sensing Technology for Transparent Power Grids: A Review

HONGYU SUN [1,2], SONGLING HUANG [3] (Senior Member, IEEE), AND LISHA PENG [3]

[1]School of Physical Science and Engineering, Beijing Jiaotong University, Beijing 100044, China
[2]Tangshan Research Institute of Beijing Jiaotong University, Tangshan 063005, China
[3]Department of Electrical Engineering, Tsinghua University, Beijing 100084, China

CORRESPONDING AUTHOR: SONGLING HUANG (e-mail: huangsling@tsinghua.edu.cn).

This work was supported in part by Tangshan Science and Technology Planning Project under Grant 23130224E, in part by the National Natural Science Foundation of China under Grant 52307001, in part by China Postdoctoral Science Foundation under Grant 2023M730207, in part by the Natural Science Talent Fund Project of Beijing Jiaotong University under Grant 2023XKRC003, in part by the Hubei Key Laboratory of Modern Manufacturing Quality Engineering Open Fund under Grant KFJJ-2023005, and in part by the Open Project of State Key Laboratory of Performance Monitoring and Protecting of Rail Transit Infrastructure, East China Jiaotong University under Grant HJGZ2023111.

ABSTRACT The global energy industry is moving toward a trend of green and low-carbon transformation. A transparent power grid represents a new development form under this energy transition trend, integrating the power grid with new generation information and communication technologies, exemplified by the Internet. The use of micro smart sensors allows real-time monitoring of many important parameters of power systems via current, which is crucial for ensuring safe, stable, intelligent, and green power grid operation. Here, based on the development logic of current sensing technology for traditional-smart-transparent power grids, we focus our research on high-current sensing in a transparent power grid. First, we review the widely used traditional current sensing methods of shunts and Rogowski coils. More advanced optical fiber current sensing methods and microelectromechanical system current sensing chips are then introduced, which are more suitable for the smart sensing requirements of transparent power grids. In addition, we present and discuss the technical characteristics, research status, application scope, advantages and disadvantages, and future development directions of the above methods in detail. Finally, we address many essential challenges, including miniaturization, integration, low power consumption, passive wireless sensing, long-range operation, and complex environmental parameters in the comprehensive intelligent and transparent sensing of current parameters in power grids. To address these challenges, we present three possible development directions: sensor improvement, development of communication and networking technologies for sensors, and the advancement of intelligent and fast processing methods through communication.

INDEX TERMS Current sensing, fiber optic sensing, magnetic field current sensing, Rogowski coil, shunt, transparent power grid.

I. INTRODUCTION

As green, environmentally friendly, and low-carbon lifestyles become popular, countries worldwide are becoming more inclined to use clean and efficient energy sources. While traditional energy systems do require and benefit from transparent power grids for reasons, such as operational efficiency, maintenance, and reliability, the urgency and benefits of such transparency are magnified in the context of renewable energy integration and the move towards a low-carbon future. As a result, the green energy industry has focused more attention on new modern power systems that can access renewable energy on a large scale. "Transparent power grid" represents an advanced form of smart grid that leverages Internet technology as a mediator, supported by cutting-edge communication technologies, and grounded in renewable energy sources. This helps to promote the energy transition, realize the vision of "carbon peak and carbon neutrality," and encourage the development of innovative power systems. In 2018, the concept of a transparent power grid was first proposed by Li Licheng, one of the authors in [1], an academician at the Chinese Academy of Engineering, in association with the Southern Power Grid Company. In 2022, this concept

was widely introduced to practitioners in the energy industry, represented by the power sector [2]. As the world is undergoing a rapid energy transformation, transparent power grids are a newly integrated form of power grid and new-generation communication technology for this transformation. The transparent power grid incorporates advanced Internet concepts and focuses on the industry's development needs while integrating information, communication, sensing, control, artificial intelligence, and other technologies within the grid. The transparent power grid's essential features include online, real-time, comprehensive awareness of the grid status, and unrestricted storage and acquisition of massive amounts of data in the grid. For instance, current and voltage sensors are used for electrical quantity data measurements, while temperature, gas, humidity, and vibration sensors are used for environmental parameter measurements. In addition, partial discharge, electromagnetic emission, and acoustic emission sensors are used for electrical equipment monitoring. Furthermore, the information transmission, operational status, and transaction status of the smart grid will always remain transparent. With the above features, the technical system of a transparent power grid can be divided into four layers: the sensing layer for information collection, the network layer for information transmission, the platform layer for information processing and decision making, and the application layer for power business scenarios [2]. The sensing layer is mainly used to construct an intelligent integrated system of Internet of Things (IoT) terminals involving multiparameter intelligent sensing. This system can perform real-time monitoring and collection of important parameters of a power system, thus improving information transparency and reliability. The construction of the sensing layer is the first and most critical step of the transparent power grid action plan.

In developing current monitoring technology, traditional current sensors, including shunts, current transformers, Rogowski coils, have disadvantages, such as environmental sensitivity, complex maintenance, large size, high cost, high energy consumption, and poor reliability. These issues make it challenging to transform smart grid research for transparent and marketable solutions. Therefore, a new type of centimeter scale smart current sensor needs to be developed to achieve more comprehensive, adequate, efficient, and reliable sensing of grid information. The development of miniature smart current sensors has focused on reducing device size and achieving a high degree of integration with self-taking energy, which significantly reduces sensor power. Therefore, it is possible to develop low-cost intelligent miniature sensors with high accuracy and reliability while achieving self-grid functionality.

In industrial applications, such as power grids, "high-current" involve currents of hundreds or thousands of Amperes (e.g., 100 to 1000 A or more) due to the high-power requirements. In transparent power grids, measuring high currents poses specific needs and challenges different from those of traditional applications. The measurement requirements and challenges in high-current applications can be described as follows.

1) *Enhanced accuracy:* Transparent power grids require high-precision current measurements for effective monitoring and control of grid performance.
2) *Sensitivity:* High-current sensing technology needs to have high sensitivity to accurately detect and measure variations in current flow for precise monitoring and control of the power grid.
3) *Wide dynamic range:* Accurate measurement of high currents within a wide range of fluctuations is essential for maintaining grid stability and optimizing power distribution in transparent power grids.
4) *Nonintrusive measurements:* High-current sensing technology should enable measurements without direct contact with power lines to ensure safety and reliability in nonintrusive monitoring of transparent power grids.
5) *Real-time monitoring:* Real-time current measurements are crucial for timely fault detection, rapid response, and effective load balancing in transparent power grids and require fast and reliable data acquisition capabilities.
6) *Environmental factors:* High-current sensing technology should be resilient to challenging environmental conditions, such as extreme temperatures and electromagnetic interference, to ensure accurate and reliable measurements in transparent power grids under varying circumstances.

From the perspective of current measurement, measurement accuracy and sensitivity are two of the most critical indicators, and the impact of dynamic range, nonintrusive measurements, real-time monitoring, and external environmental changes should also be considered. Current sensors play an important role in grid state monitoring, automation control, and fault detection scenarios. However, the development of existing power grids is already approaching the pinnacle of smart grids. It is not only necessary to adapt to the wide-range, wideband, and highly reliable current monitoring requirements of traditional grids but also necessary to transition toward more advanced intelligent, market-oriented, and IoT-based transparent grids to achieve comprehensive intelligent and transparent perception of grid states. In this regard, miniaturization design, low-power-consumption measurement, intelligent control, and reliable communication of current sensors are important performance requirements. Therefore, in the future, improvements in current sensor performance need to encompass three areas: sensor improvement, development of communication and networking technologies among sensors, and advancement of intelligent and fast processing methods through communication.

Considering the above aspects and based on the development route of current-sensing technology in traditional smart transparent power grids, we present an overview according to the logic of Fig. 1. As shown in this figure, the traditional measurement of current in the power grid relies on shunts, current transformers, and Rogowski coils. However, these methods have drawbacks, such as large sensor sizes, low measurement sensitivity, and difficulties in nonintrusive measurement. In contrast, smart power grids, characterized by

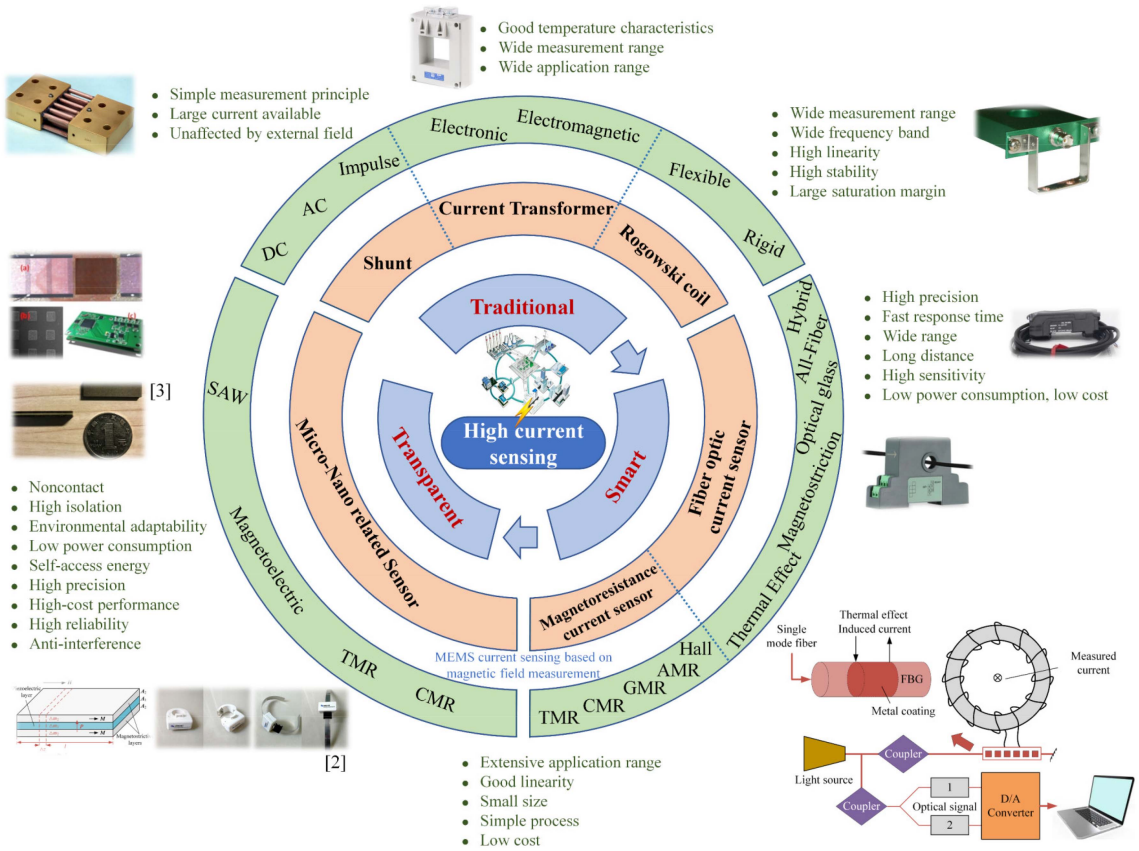

FIGURE 1. **Framework for current sensing methods based on traditional-smart-transparent power grid logic [2], [3], [109].**

informatization, automation, and interactivity, mainly adopt methods, such as magnetic resistance and optical fiber current sensing. These methods significantly reduce the sensor size, further improve the detection sensitivity, and enable reliable noncontact measurement of the current. A transparent power grid relies more on intelligent micro/nanocurrent sensing methods for current measurement. These methods include surface acoustic waves (SAW), TMR, CMR, and magnetoelectric (ME) sensing. In this article, the measurement principles, development history, technical characteristics, application scope, advantages and disadvantages, and future development directions of high-current sensing technology, including traditional current shunts, Rogowski coils, and new fiber optic and magnetic field microelectromechanical system (MEMS) current-sensing technology, are reviewed and outlined.

II. CURRENT SHUNTS

As a type of current sensor widely used in ac/dc transmission and power metering in power systems, as well as renewable energy generation, electric vehicle charging stations, and industrial power monitoring in the transparent grid scenario, the current shunt has the advantages of a simple measurement principle and structure, a high measurable current (especially for impulse shunts), and low cost. As early as 1889, Weston obtained a patent for a compensating resistive material and subsequently developed a current measurement method based on a manganese–copper alloy resistive shunt. This Ohm's law-based current measurement method essentially relies on the working principle of a resistor: when the current flowing through a resistor increases, so does the voltage across it, and thus, the current magnitude can be obtained. To reduce the measurement error of high currents up to several tens of kiloamps (kA), a shunt, generally having a four-terminal structure including two current input terminals and two voltage output terminals, is used. This is because in a four-terminal shunt, virtually no current flows through the voltage leads, meaning the impact of contact resistance and lead resistance on the voltage measurement is negligible. This implies that the voltage drop measured across the terminals of the voltage output more accurately reflects the actual voltage drop caused solely by the current passing through the shunt, thereby eliminating errors introduced by additional resistances in the circuit. Chips or rod resistors are generally made of manganese–copper material, with resistance values generally ranging from milliohms to ohms.

Therefore, based on the above theory, the shunt needs to be connected in series in the circuit under test to obtain the current measurement; that is, this approach is a contact current-measurement method. However, different types of

TABLE 1 Performance Comparison of Current Shunts

Method	Amplitude (kA)	Frequency (kHz)	Cost	Disadvantages	Advantages
DC Shunt [3], [4], [5], [6]	10	-	Low	Relatively high-temperature coefficient, complex insulation, low sensitivity	Low price and good linearity
AC Shunt [7], [8], [9], [10], [11], [12], [13], [14], [15]	0.1	0.01–10	High	Poor overload capability, poor high frequency high current measurement, expensive	AC measurement
Coaxial Tube Impulse Shunt [17], [18], [19], [20]	100	1.2×10^5	High	High cost, large size	Wide application, simple structure, simple principle
Squirrel Cage Impulse Shunt [21], [22], [23]	100	10	Low	High rise time requirements needed to match the compensation circuit at the output	Suitable for measuring high-amplitude currents and obvious heat generation effects
Flat strap Impulse Shunt [24], [25], [26]	100	1000	Low	Large residual inductance, difficult to measure impulse currents with bandwidth less than 10 ns	Low influence of external magnetic fields, small-loop inductance, excellent square wave response characteristics, small size
Disc-Type Impulse Shunt [27], [28], [29]	0.1	3×10^5	Low	Difficult to apply to DC systems above 100 kV	Slight temperature drift, wide frequency band, good heat dissipation, can shield external magnetic field interference

shunts have different structures and rated parameters that need to be considered based on the characteristics of the measured current. For example, when measuring ac current using a shunt, the presence of parasitic inductance and capacitance in the shunt needs to be considered due to frequency variation. This becomes even more prominent when measuring impulse currents. Therefore, in the design of an impulse shunt, factors, such as the distributed capacitance and inductance, skin effect, thermal effects, and mechanical strength, need to be considered. As a result, we prefer to classify shunts into three categories, dc, ac, and impulse shunts, to reflect the additional considerations required for each type of shunt based on the specific measurement requirements; these are given in Table 1, and we review their development status.

A. DC SHUNTS

DC shunts for dc measurements have been widely used in power grids and industrial instruments, especially in current transformers in dc transmission systems, where their measurement accuracy in industrial scenarios can reach the 0.5 to 2 level, representing a measurement error between 0.5% and 2%. In addition, they perform well in dc measurements below 10 kA. This is because considering thermal management, long-term stability, and safety, using a dc shunt to measure currents exceeding 10 kA is not suitable. A schematic diagram of the principle and structure of a dc shunt at different rated currents is shown in Fig. 2. The difference between a two-pin current shunt and a four-pin current shunt in Fig. 2(a) is typically related to the current load. Generally, current shunts with a current load less than 500 A typically use two pins, while those with a load above 500 A usually use four pins. Additional pins for higher current shunts are needed to handle the larger current load, provide better current conduction, and improve the heat dissipation capabilities. Depending on the rated current of the shunt, its power consumption can reach several watts to several hundred watts, and the temperature of the resistor body may exceed 320 K. Thus, this device can have a significant impact on measurement accuracy in high-current detection. To solve the many problems caused by temperature drift, scholars have studied three main perspectives: signal processing algorithms, shunt structure design, and resistor material properties. First, Kraft investigated the self-heating effect and error of a manganese–copper dc shunt sheet from the perspective of signal processing algorithms, calculated the time required for the shunt to reach temperature equilibrium and resistance equilibrium, and reduced the measurement error with symmetrical, low-resistance connections [4]. In industrial practice, the ambient temperature often varies over a broader range, and the effect of temperature on measurement accuracy becomes increasingly obvious. Immersion of resistors in flowing insulating oil is a viable option for reducing the effects of a temperature increase. However, this approach poses new problems; that is, keeping shunts in oil is not conducive to service and maintenance, the system cost is considerably greater, and installation is cumbersome. An alternative approach to address temperature effects is to use epoxy instead of hard grease to modify manganese–copper resistors, supplemented by a resistance temperature calibrator; this method can reduce the measurement uncertainty by more than five times and is simpler and easier to implement than the oil immersion method. In addition to algorithmic temperature coefficient compensation, Kato et al. [5] proposed a modular high-current measurement scheme in terms of shunt structure improvement; i.e., two layers of sensors are arranged to perform different functions. Specifically, the upper layer is a measurement circuit with a temperature measurement function used to correct the shunt resistance in real time,

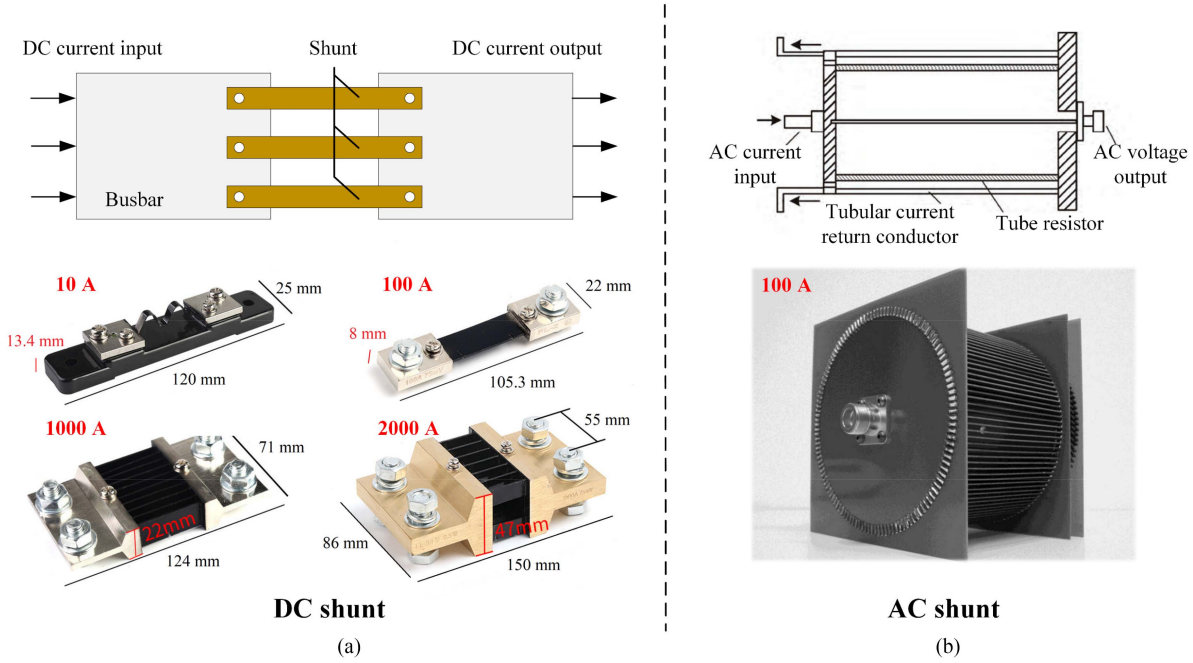

FIGURE 2. **Schematic diagram of dc and ac shunts. (a) DC shunts with different current ratings. (b) Coaxial ac shunts [12].**

and the lower layer comprises potential terminals of multiple shunts connected in parallel. Subsequently, the data acquisition unit can pool the measurement data from each branch to calculate the total current. Experimental studies have shown that the error of the proposed method is less than 0.5% for a 1-kA current measurement under full temperature range conditions [5]. Moreover, the material properties of resistors, including nichrome (nickel, chromium, and soft iron alloys), manganese–copper (84% copper, 12% manganese, and 4% nickel alloy), Kang copper (55% copper and 45% nickel alloy), and white copper [6] alloys, have also been considered to suppress temperature drift by focusing on the low-value constant characteristics of the temperature coefficient. After measurement, it was found that Ni–Cr alloys had the highest resistivity ρ (1.33×10^{-6} Ω·m, 293 K) and the lowest temperature coefficient α (20×10^{-6} K^{-1}; the same was true for manganese–copper alloys), and white copper had the lowest resistivity (0.23×10^{-6} Ω·m, 293 K) [7]. All these materials have small and approximately constant temperature coefficients α and can be used selectively in dc shunts according to practical needs.

B. AC SHUNTS

Unlike dc measurements, when a shunt is used for ac measurements, additional consideration needs to be given to the effect of frequency changes on the shunt impedance parameters due to parasitic inductance and capacitance in the shunt. In addition, there is a skin effect of the current in the resistor at high frequency. This effect reduces the cross-sectional area available for current flow, which can increase the apparent resistance of the conductor. In addition, complex inductance and capacitance characteristics in resistors at high frequencies lead to a phase shift of the output voltage of the ac shunt, reducing its measurement accuracy. Commonly used ac shunt structures include coaxial squirrel-cage structures. Most existing studies have focused on reducing the effects of spurious parameters and shunt temperature increases, as well as analyzing the mechanical stresses on the resistor body, to improve the measurement range of the ac frequency and amplitude and reduce measurement error [8].

Early high-frequency current measurement methods based on manganese–copper resistors generally involved the use of coaxial ac shunts, as shown in Fig. 2. For example, a dc–ac 100 kHz coaxial shunt was designed at Argonne National Laboratory; this shunt enables both dc and ac measurements and can operate uninterruptedly with a power consumption of 24 kW. The measurement uncertainty of the device at 100 A and 100 kHz ranges from 4×10^{-5} to 1.0×10^{-4}. This shunt is generally used in high-grade calibration laboratories for quantity traceability and precision electrical energy measurements [9], [10]. On this basis, squirrel-cage structures suitable for commercial ac shunts are more common [11], [12]. This open parallel structure can effectively improve the ac current measurement range and accuracy. However, its high cost and temperature effects are not negligible, so its accuracy needs to be evaluated by corresponding standards and methods, such as magnetic bridge current sensors and electronic current transformers [13], [14]. To evaluate the frequency and current dependence of shunt resistors at different ac levels, a modified current-bridge method was developed by Dianov [15] based on 100 squirrel-cage shunt resistors connected in parallel with 10 Ω foil resistors. The researcher investigated the influence

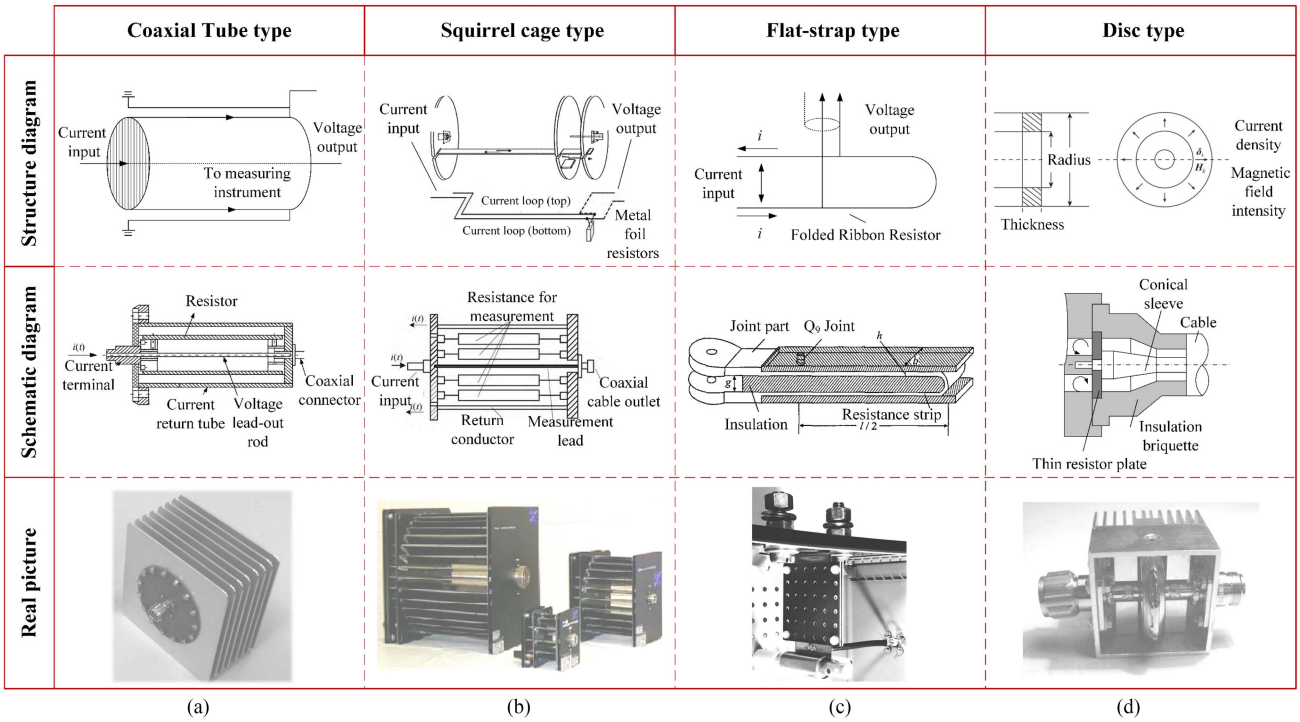

FIGURE 3. Principles, structures, and physical diagrams of different types of impulse shunts. (a) Coaxial-tube type [28]. (b) Squirrel-cage type [5]. (c) Flat-strap type [25]. (d) Disc type [28].

of the temperature rise of resistors at different ac on the uncertainty of the current measurement, thus extending the shunt's measurement frequency and current range [15].

C. IMPULSE SHUNT

An impulse shunt is a unique ac shunt that is generally used to measure current pulse signals with high amplitude along short rising edges [16]. Due to its advantages of simple principles, robustness, high accuracy, and controllable cost, the impulse shunt is widely used in controlled nuclear fusion tests, electromagnetic railgun condition monitoring, and material surface treatment. Furthermore, impulse shunts are used mainly in power systems for accurate measurement of short-circuit currents and lightning currents and thus have important scientific significance and application value. Generally, the amplitude of an impulse current can reach tens to hundreds of kA, and the rise time can reach the microsecond or even nanosecond level; therefore, in contrast to the ac shunt, it is necessary to fully consider the distributed capacitance inductance, skin effect, thermal effect, mechanical strength, and other factors during current measurements using an impulse shunt. First, the voltage drop of the residual distributed inductance is positively correlated with the rate of change in the current. This means that the step response of the shunt will hinder the determination of the waveform and amplitude of the upstroke. In addition, when an alternating current flows through the shunt, it will be unevenly distributed within the conductor due to the skin effect, which will cause the impedance of the shunt to change, and the thermal effect will further lead to amplitude error and waveform distortion of the voltage output. Moreover, the stability and mechanical strength of the shunt at high frequency and high current also need to be fully considered.

To accommodate the trend of increasing impulse current amplitude and shortening rise time, scholars have proposed various shunt structures to optimize the bandwidth parameters and enhance the response characteristics since the distribution parameters, temperature increase, and mechanical strength of shunts are mainly affected by their structures. In this section, the existing structures of shunts are divided into four types: the coaxial-tube, squirrel-cage, folded-band (flat-strap), and disk types, as shown in Fig. 3; their development status is also reviewed.

1) COAXIAL-TUBE IMPULSE SHUNT

The measurement of impulse current has high requirements regarding the bandwidth parameters of an impulse shunt. Reducing the parasitic inductance of the shunt as much as possible can effectively increase the upper cutoff frequency, but the magnitude of the parasitic inductance is related to the mutual inductance between the current and voltage loops. Therefore, to reduce the parasitic inductance of the shunt, an impulse shunt structure in the form of a coaxial tube can be used. This structure exploits the nature of the equal amplitude and opposite direction of the current in the resistive inner cylinder and the outer shielded cylinder so that the magnetic field between the inner and outer cylinders is approximately zero, thus widening the measurement bandwidth

of the impulse current while reducing the parasitic inductance [17]. Fig. 3(a) shows the schematic structure and current flow direction of a coaxial tubular impulse shunt, where the wall thickness of the resistor body is usually on the order of microns to reduce the skin effect. The desired resistance and temperature increase determine the parameters, such as the length and number of roots of the resistor body.

In a study on coaxial tubular impulse shunts, Liu et al. [18] from the National University of Defense Technology designed a high-current coaxial impulse shunt with a nanosecond rising edge, in which the resistor is composed of a coil of 80 μm thick Kang-Cu with a 5 mm radius core rod and a Qg-type cable structure at both ends. The current to be measured passes through a small resistor barrel to generate a voltage drop. This shunt enables effective measurement of pulsed currents up to 40 kA with a square-wave rise time of 3 ns and a measurement uncertainty of less than 3% [18]. Filipski et al. [19] of the Austrian National Institute of Metrology proposed a four-barrel coaxial metal film structured shunt, which included a manganese–copper foil resistor barrel, a copper foil current return barrel, and a high-voltage lead-in barrel. These three cartridges are insulated from each other with a glass fiber epoxy core, and a large cartridge core and thick input and output plates are used to ensure the mechanical strength of the impulse shunt. The shunt can measure impulse currents up to 100 A and 100 kHz with low measurement uncertainty, namely, no more than 20 $\mu\Omega/\Omega$ at 20 kHz and no more than 40 $\mu\Omega/\Omega$ at 100 kHz [19]. Sakharov et al. [20] from the All-Russia Research Institute of Optophysical Measurements designed a coaxial bellows-type shunt for measuring a 200-kA impulse current amplitude. The impulse shunt has a resistance of 1.25 mΩ, a rise time of 104 ns, and a measurement uncertainty of 4.2%. This bellows-type structure allows the transient response rise time of the impulse shunt to be sufficiently small by extending the resistance length of the shunt and reducing the wall thickness to 0.5 mm without adding additional inductance, while retaining sufficient strength to resist tensile compression and deformation due to electrodynamic forces [20].

2) SQUIRREL-CAGE IMPULSE SHUNT

The squirrel-cage shunt is formed by variation of the coaxial tube shunt. As shown in Fig. 3(b), the squirrel-cage impulse shunt uses multiple resistors connected in parallel. The resistive elements are soldered to two end faces of a strip printed circuit board (PCB), and the current returns to the low-potential end face of the input through the other side of the PCB after flowing through the resistive elements. This shunt is advantageous in measurement situations with high currents and significant heat generation. However, the mutual inductance between the parallel resistors makes it challenging to measure nanosecond lightning impulse currents effectively, and matching compensation circuits at the output are required to suppress the overshoot caused by large inductances [21]. Since 1990, when the design idea of the coaxial squirrel-cage shunt was proposed by scholars at the Russian Institute of Metrology (VNIIM), to 2000, when the prototype 20-A squirrel-cage shunt was developed by Rydler at the Swedish National Institute of Metrology, many scholars have investigated its current measurement characteristics.

Sanoh et al. [22] developed a coaxial-cage-structure impulse shunt as a new standard test instrument for the Agilent Technologies Metrology and Standards Center, Japan. This shunt uses 80 commercial high-precision, low-temperature-coefficient foil resistors with a nominal resistance of 5 mΩ in parallel as the main structure of the shunt to achieve accurate measurements of large currents up to 1500 A. The measurement uncertainty of this shunt is 0.035% at a current amplitude of 400 A and a pulsewidth of 1 ms. Fluke, USA, designed and manufactured the A40B series of precision impulse shunts based on the patented coaxial-cage shunt of the Technical Research Institute of Sweden, which can measure currents from 0.0001 to 100 A and bandwidths from dc to 100 kHz, with annual stability and ac/dc differences of 10^{-5}. Ferrero et al. [23] of Politecnico di Milano, Italy, developed an inductance–resistance resolution model of a double-layer squirrel-cage shunt (resistance = 70.9 Ω, inductance = 5.01 nH, rise time = 70.9 μs) under an impulse current to further improve the shunt bandwidth from a design optimization point of view; these researchers achieved effective measurement of high-frequency impulse currents at 2 MHz.

3) FLAT-STRAP IMPULSE SHUNT

The principle of this type of shunt is similar to that of the coaxial-tube-type impulse shunt. As shown in Fig. 3(c), the input current terminal is connected in series with the measured loop, so the current flow on the two sides of the flat-strap resistor body is reversed, and the loop inductance is significantly reduced, thereby increasing the measurement bandwidth. In addition, when the loop area formed by the output lead and shunt is smaller, the influence of the external magnetic field is also lower, thus enabling accurate kA measurements and nanosecond-level rise time impulse currents [24].

In 1999, Castelli [25] of Politecnico di Milano, Italy, first proposed an ultrathin flat-strap surge shunt structure with a band resistor sheet thickness of only 25 μm to ensure a uniform current density distribution. It was shown that the response time, power consumption, and frequency characteristics of the designed ultrathin flat-strap shunt structure were better than those of the coaxial shunt. In addition, the structure is simple and inexpensive to process and can be used to measure large impulse currents up to 10 kA and short-rise-time lightning currents of less than 3 ns, significantly reducing proximity and skinning effects [25]. On this basis, Liu et al. [26] of the National University of Defense Technology proposed a more compact flat-strap impulse shunt, which has a resistance band of 0.02×80 mm^2 stainless steel with a gap of 6 mm. This device saves installation space while increasing the amplitude of the measurable impulse current to 50 kA.

However, the residual inductance of this shunt is large, making it difficult to measure impulse currents with a rise time of less than 10 ns [26].

4) DISC-TYPE IMPULSE SHUNT

The most widely used tube shunts suffer from a contradiction between structure length and volume for high impulse currents. As a result, they cannot simultaneously meet the measurement requirements of long duration and short response time. In addition, compared with the equivalent wavelength, the length of the resistive tube at very high frequencies cannot be neglected and cannot be analyzed by the centralized parameter method. Therefore, scholars have proposed a planar-type disk shunt with a low inductance and a short rise time, as shown in Fig. 3(d). The resistance of this disk-type impulse shunt is usually applied at the end of the coaxial transmission line. Accurate measurement of a short-rise-time current can be achieved by extracting the voltage signal at the center and edge of the disk.

Yu and Yu [27] of Xi'an Jiaotong University developed a disk shunt that can measure very short rise time currents with a disk-shaped resistive film designed with a thickness of 10 μm. The shunt is connected to a coaxial cable through a conical barrel, allowing the measurement of 0.3 ns rise time currents, and its square wave response characteristics were investigated [27]. Pogliano et al. [28] of Istituto Nazionale di Ricerca Metrologica, Italy, designed a disk shunt for ac–dc current transmission standards to improve the accuracy of ac measurements over a wide frequency range. However, the design of the above shunt is only in the prototype stage, and it is not easy for it to measure large currents above tens of amperes. Zhang et al. [29] of the Beijing Institute of Radio Metrology and Measurement proposed a disk shunt suitable for large impulse currents. This shunt has the advantages of a small temperature drift, a wide frequency band, good heat dissipation, and shielding from external magnetic interference. It can accurately measure currents up to 100 A with an accuracy of 0.1%. The disk shunt has a resistance of 0.01 Ω and can measure short-rising-edge impulse currents from 0.05 to 10 kHz [29].

D. SUMMARY

Current-sensing technology based on shunts requires a calibrated, high-precision resistor to be connected to the circuit, and the voltage drop across the resistor reflects the amplitude of the measured current. Shunts have the advantages of a simple measurement principle, no external magnetic field influence, and high accuracy, so they can be used for value traceability and precision power measurements in high-level calibration laboratories. However, shunts need to be installed in the main circuit so that they can affect the electrical parameters of the circuit. In addition, primary and secondary circuits are directly connected electrically, which has a significant impact on the high-frequency and high-power switching power supply, control and protection system safety applications. Furthermore, the temperature drift of the shunt, residual inductance, and impact of the skin effect can reduce the accuracy of shunt measurements and should not be ignored.

DC shunts are the most widely used commercial current-measurement products in the industrial field. These products can achieve precision measurements of large direct currents of tens of kA. However, the dc shunt temperature drift can severely impact current measurements. Improved solutions include advanced algorithm compensation, a good heat dissipation structure, and the selection of low-temperature-coefficient resistor materials.

AC shunts are less commonly used for high-current measurements but are highly accurate for 100 kHz ac measurements below 100 A. However, ac shunts need to consider the influence of both the temperature drift and the frequency change on shunt impedance parameters. Hence, the manufacturing cost is generally high, but adopting a coaxial and squirrel-cage ac shunt structure can address the above problems to a certain extent.

An impulse shunt is a unique ac shunt that can measure a large impulse current with a short rising edge of 100 kA. Compared with the accuracy of the amplitude measurement, the time response characteristics are more important. Surge shunts have the advantages of simple principles, high robustness, high accuracy, and controllable cost. However, they also face the problems of residual inductance, skin effects, and thermal effects, resulting in a reduction in current detection accuracy and mechanical stress stability under surge currents. The coaxial-tube, squirrel-cage, and flat-strap shunts can detect a 100-kA impulse current accurately. In contrast, disk-type shunts have more advantages regarding the measurement bandwidth. Specifically, these devices can accurately measure 3-MHz ultrashort-rising-edge impulse currents but cannot easily measure large currents at the kA level. Regardless of the structure of the impulse shunt, the design goal is to minimize the residual distribution inductance to improve the measurement bandwidth. These shunt structures include the more widely used coaxial-tube and squirrel-cage types, while the flat-strap and disk-type structures are still in the testing and development stage.

III. ROGOWSKI COIL

With the rapid development of transregional ultrahigh voltage grids that are connected to a large percentage of new energy sources, the demand for measuring steady-state ac, transient, and impulse high currents has been increasing in many application scenarios in power systems. These scenarios include transmission line short-circuit current measurements, distribution cabinet current detection, power equipment high-voltage insulation testing, lightning overcurrent measurements, controlled series complementary capacitor current detection, and switching current monitoring of power electronics. Although the shunts introduced in the previous section can measure such high currents, the shunt affects the electrical parameters of the

TABLE 2 Performance of Rogowski Coils

Method	Amplitude (kA)	Frequency (kHz)	Cost	Disadvantages	Advantages
Rogowski Coil [30],[31], [32],[33],[34]	1000	10 000	High	Unable to measure DC	Good linearity, wide range

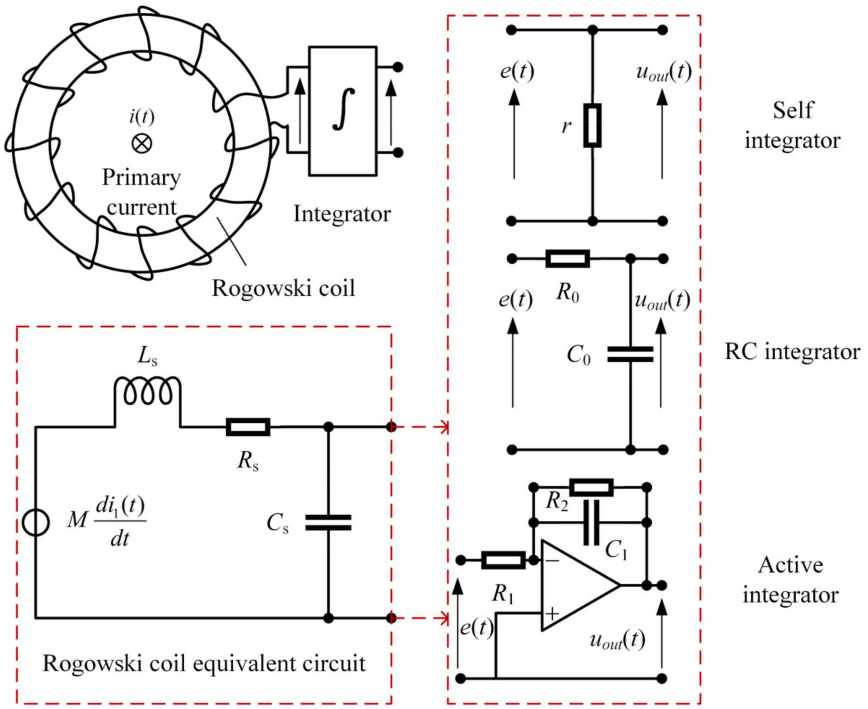

FIGURE 4. Schematic diagram of the structure of a Rogowski coil and a concentrated-parameter equivalent circuit diagram with different kinds of integral circuit structures [41].

current loop being measured when it is connected to the primary circuit. There is no electrical isolation between the primary and secondary circuits, so the measurement error is large and there is low safety. A current transformer that can convert a large current to a small current effectively solves the electrical isolation problem and is widely used in power systems [30]. A traditional electromagnetic current transformer can meet the basic needs of power system measurements. However, its insulation structure is complex and expensive, and the core saturation effect is large, so it is difficult to adapt to modern power systems because of intelligent and automated control and protection equipment requirements. Advanced electronic current transformers have the advantages of low cost, no magnetic saturation, strong anti-interference, small size, and light weight, and their output signals can be directly connected to an intelligent sensing system, which adapts to the development needs of digitalization and automation of power systems [31]. The Rogowski coil, as a differential electronic current transformer for steady-state ac, transient, and impulse high-current measurements, was proposed by Rogowski and Steinhaus [32] as early as 1912. With the advantages of good electrical insulation, wide measurement range, high accuracy, easy digitization, and high safety [33], Rogowski coils have been used more often in power system relay protection, series arc fault detection, harmonic testing, thermonuclear fusion, and plasma physics [34]. In this section, we will review the existing methods for modeling Rogowski coil circuits; review electromagnetic interference weakening methods based on the detection principles and types of Rogowski coils, as shown in Table 2; summarize the deficiencies and challenges in existing research; and provide possible solution ideas.

A. MEASUREMENT PRINCIPLES AND CLASSIFICATION

Although the design parameters of the Rogowski coil, such as sensitivity, shape, and size, differ depending on the characteristics of the measured current, conductor structure, and application conditions, its fundamental operating principle is the same [35]. As shown in Fig. 4, the basic structure of the Rogowski coil is a toroidal skeleton made of nonferromagnetic material according to Faraday's law of electromagnetic induction and Ampere's law. The measurement coil should

return to the starting point after progressing along the circumference of this skeleton [36].

$$u_s(t) = M\frac{di_1(t)}{dt} \tag{3.1}$$

where u_s is the open-circuit voltage across the Rogowski coil, M is the mutual inductance between the conductor under test and the coil, and i is the current. The above equation does not consider the effect of parasitic capacitance inductance on the output voltage and is applicable only at low current frequencies. The integration circuit on the right-hand side is used to reduce the output of the induced electromotive force of the Rogowski coil with respect to the measured ac. According to the integration principle, Rogowski coils can be divided into the following three categories. The Rogowski coil's centralized parametric equivalent circuit is shown in Fig. 4 on the left, and three different integration circuits are shown on the right. First, the self-integrating method requires access to only a noninductive resistor at the coil terminals to achieve infinite-bandwidth current sensing. However, this method has a small gain, a high error rate, and an impedance mismatch, which leads to oscillation at the coil resonant frequency [37]. Second, the passive integration method requires access to an RC integrator to measure the coil's induced voltage, which has a cutoff frequency of $f_0 = (2\pi R_0 C_0)^{-1}$ and is valid only above f_0 [38]. Finally, active integrators containing analog operational amplifiers have more stable components and termination parameters. Unlike those of passive integrators, the input and feedback signals of inverting-type op amps are located at their negative inputs, which may cause waveform distortion. In contrast, the in-phase integrator does not draw current from its input, which flows through all its resistors and capacitors; thus, an RC circuit can be introduced to avoid capacitive coupling of the output. The above integrator is also referred to as an active integrator [39].

Supported by the above measurement principles, Rogowski coils can be divided into three categories according to the characteristics of the coil and skeleton, as shown in Fig. 5.

The traditional flexible coil winding form is widely used to measure the current in large or irregular conductors. However, ensuring the uniformity of the coil winding is difficult, and the measurement accuracy is not high [40]. Rigid PCB-based Rogowski coils effectively solve the problem of low coil uniformity and effectively reduce the coil size, making them easier to integrate into small devices. This approach also significantly reduces manufacturing and processing costs by producing a coil with a uniform turn distribution without the need for expensive winding machines, making it suitable for high-current, wideband measurement applications. Furthermore, to further broaden the use of PCB-based Rogowski coils, flexible printed circuit (FPC) processing technology with a flexible backbone was introduced, which has a promising future despite its high manufacturing cost [41].

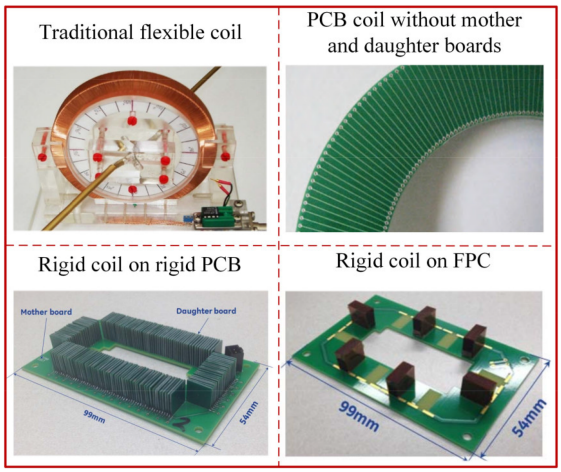

FIGURE 5. Classification of Rogowski coils according to the characteristics of the coils and skeletons: a conventional flexible coil [42], a PCB coil without mother and daughter boards [7], a rigid coil on a rigid PCB, and a rigid coil on an FPC [43].

B. COIL CIRCUIT MODEL

In low-frequency current measurements, the mutual inductance between the Rogowski coil and the conductor determines the measurement sensitivity and immunity of the Rogowski coil [44], [45], [46]. Moreover, when the measured current frequency is high, the sensitivity of the Rogowski coil is additionally affected by the parasitic capacitance and inductance inside the coil. Consequently, the accurate calculation of these parameters primarily affects the accuracy and sensitivity of the current measurement [47], [48]. Therefore, effective modeling of Rogowski coils is essential for their development and design.

The centralized parametric model is the simplest and most widely used model for low-frequency current measurements, as shown in Fig. 4. The model includes the winding resistance R_s of the coil, the inductance L_s, the mutual inductance factor M, and the capacitance to ground C_s [40], [49]. Given the tight and uniform winding of Rogowski coils, their ground capacitance is dictated by the coil's diameter and the geometrical configuration of the winding, with the wire diameter's contribution being relatively minor.

$$R_s = \frac{\rho_c l_w}{\pi d^2} \tag{3.2}$$

$$L_s = \frac{\mu_0 N^2 w}{2\pi}\log\frac{b}{a} \tag{3.3}$$

$$C_s = \frac{2\pi^2\varepsilon_0(a+b)}{\log[(b+a)/(b-a)]} \tag{3.4}$$

where l_w, d, and ρ_c are the length, radius, and resistivity of the wire, respectively; w is the toroid width; N is the number of turns of the coil; a and b are the inner and outer radii of the coil, respectively; and $M = L_s/N$. Tao et al. [50] directly measured the specific values of each parameter in the centralized parametric model via an impedance

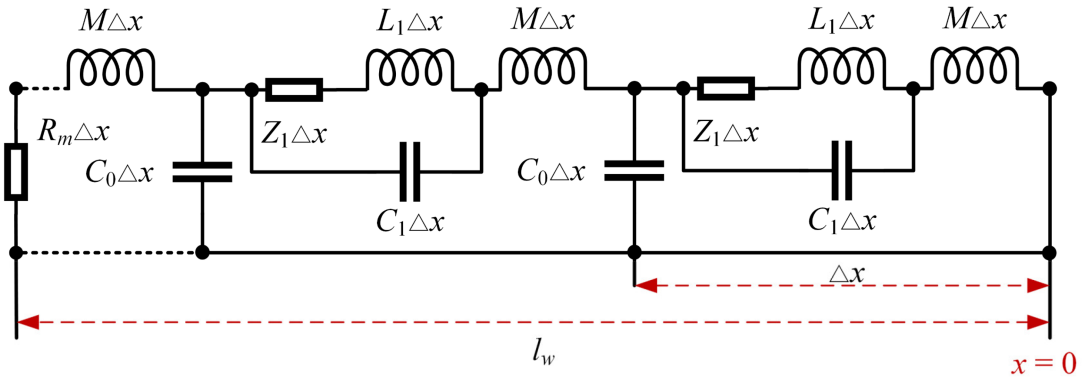

FIGURE 6. Distribution parameter model of Rogowski coils [41].

analyzer to reduce the measurement error when the above equations consider skinning and proximity effects at high frequencies. This direct measurement method ensures the accuracy of the parameters but requires expensive equipment [50]. In the indirect measurement method, Shafiq et al. [51] used the fast Fourier transform method to calculate the coil's resonant frequency, from which the coil's capacitance and inductance were calculated. However, in addition to the calculation complexity, the coil's self-impedance cannot be obtained via this method; therefore, this approach is difficult to use in a generalized way. Hence, the centralized parametric model of Rogowski coils at high frequencies faces problems, such as expensive measurement equipment and complex algorithms. A simplified centralized parametric model with lower accuracy is still required for a specific error tolerance range.

The distribution parameter model provides a better solution for modeling long coils and high-frequency Rogowski coils when the wire turns are sparsely or more uniformly distributed, as shown in Fig. 6. Here, $\triangle x$ is the calculated unit length, R_{m} is the port resistance, M is the distributed mutual inductance between the conductor and the Rogowski coil, C_0 is the Rogowski coil's distributed capacitance to ground, Z_1 is the distributed internal impedance of the Rogowski coil under the skin effect, C_1 is the distributed capacitance of the wire turns to ground, L_1 is the winding self-inductance, and l_w is the wire length. However, this distributed parameter model is difficult to apply in PCB Rogowski coils with traces and through-holes. To address this issue, Guillod et al. [52] proposed a partial-element equivalent circuit method that can extract the parameters of the equivalent circuit of the PCB coil geometry, the bandwidth of the coil, the measurement sensitivity, and the sensitivity to interference currents. Furthermore, in their study of transient and pulsed current measurements using PCB Rogowski coils, Hewson and Aberdeen [53] performed a distributed calculation of the inductance of individual magnetic channels and through-hole distributions. These researchers then summed them into segments to calculate the self-inductance of the coil [53]. Despite the prevalence of computational errors in the above methods, they generally have higher accuracy than the centralized parametric model.

As the application of PCB Rogowski coils has expanded, the coil structure has been redesigned, including rectangular-turn Rogowski coils that do not possess symmetry. Therefore, it is essential to model these complex structures of PCB Rogowski coils accurately. Ibrahim and Abd-elhady [54] investigated the modeling method for calculating the mutual inductance coefficient between the coil and the long straight wire based on two rectangular skeleton cross-section PCB Rogowski coil structures. The authors experimentally obtained the frequency response law of the coil. Habrych et al. [44], on the other hand, evaluated the current measurement performance of multilayer spiral PCB rosette coils from power system current transformers and obtained fitted models of coil self-inductance, parasitic capacitance, and resistance. Lesniewska and Lisowiec [55] used a 3-D field path finite element modeling method to analyze the effect of external magnetic fields on multilayer high-density PCB Rogowski coils. The above modeling methods can provide general guidance for designing PCB Rogowski coils, including parameters, such as coil turns, shape, and material, to achieve an optimal compromise in terms of improving the measurement bandwidth and sensitivity of Rogowski coils.

C. AVOIDANCE OF ELECTROMAGNETIC INTERFERENCE

Far-field radiation from the varying magnetic fields of other current-carrying conductors and near-field coupling from the rapidly varying electric fields of nearby power semiconductor devices can affect the detection accuracy of Rogowski coils in engineering practice. In general, the former usually employs additional wire loops to counteract the induced voltage generated by the same radiated interference, while the latter can be used to eliminate the high-frequency voltage component by adding shielding [56].

In many studies, return loops have been used to eliminate far-field radiation interference in various structural forms of PCB Rogowski coil design methods, as shown in Fig. 7. The early PCB coil structure was relatively simple, as shown in Fig. 7(a), where the solid line and the lower dashed red

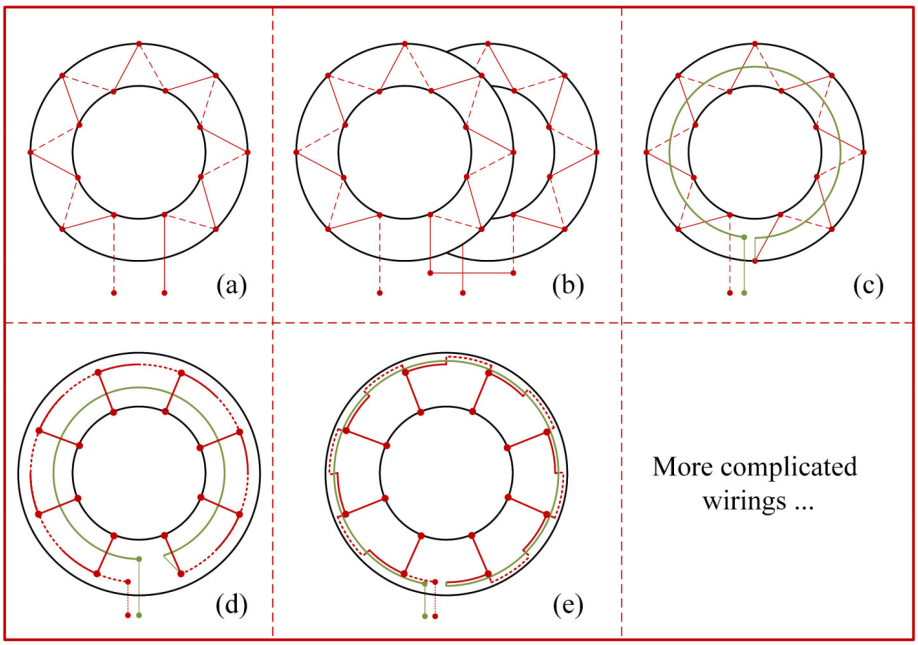

FIGURE 7. Winding methods for PCB Rogowski coils. (a) Conventional single coil. (b) Dual coil, which can reduce electromagnetic interference. (c) Return-loop method. (d) Symmetrical return-loop method. (e) Improved symmetrical return loop method [41].

trace were connected by through-hole points to form rectangular coil turns. However, this coil structure is not resistant to far-field electromagnetic interference [57]. Placing another Rogowski coil with opposite coil windings near the first coil is a feasible solution for attenuating radiated interference. As shown in Fig. 7(b), the external magnetic field under this structure induces the same voltage amplitude but opposite polarity in the two coils, and thus, they cancel each other out. Although this dual-coil structure is easier to implement, it has a high number of turns, high operating power consumption, and high cost [58]. Therefore, to solve the above problems, the return-loop method was introduced in the structural design of the anti-teleportation Rogowski coil, as shown in Fig. 7(c), where the green wire starts at the end of the coil, reverses one turn along the coil loop, and leads out from near the first end, forming two outputs. However, due to the asymmetry of the top and bottom traces, the areas enclosed by the loop and the coil are not equal, which reduces the ability to eliminate interference [59]. Tao et al. [50] proposed a symmetric trace structure to address this problem, as shown in Fig. 7(d). However, this approach still does not solve the consistency of the area enclosed by the loop and the coil, i.e., the magnetic flux area is still not equal, and the error is large. Therefore, these investigators proposed a structure, as shown in Fig. 7(e), to solve the problem entirely. Similar compact PCB Rogowski coil structure designs were also implemented by Fritz et al. [60] to weaken the radiated magnetic field interference. However, these structures are generally complex and difficult to implement [60]. Therefore, either a simple and easy-to-implement far-field radiated interference cancellation strategy needs to be developed, or a tradeoff between effectiveness and cost needs to be made.

Shielding technology is critical in near-field coupling suppression and is an effective way to isolate rapidly changing electric fields at the near end. In the conventional design of wire-wound Rogowski coil shields, as shown in Fig. 8, Cheng et al. [61] tested and simulated the shielding effectiveness of a common C-shaped metal housing. These researchers found that electromagnetic interference passes through a housing and enters the interior through gaps in the inner wall and that shielded housings with a larger ratio of inner diameter to height had worse performance [61]. Similar deficiencies have been found in many existing studies of multilayer cylindrical shielding [62], axisymmetric multilayer composite shielding [63], and small-size housing shielding [64]. In the PCB Rogowski coil shielding design, shielding can be achieved by using two external layers of PCB coils, as shown in Fig. 8. The winding and shielding are designed on a six-layer PCB, with the internal four-layer winding formed by traces and through-holes and the shielding placed on the top and bottom layers. Since the shield is used only to shield the electric field and not the magnetic field associated with the mutual inductance M, the top and bottom shield traces are connected only at a single common connection [65]. Therefore, although near-field coupling effects cannot be avoided in applications such as high-frequency turn-on of high-power power electronics, the effect of near-field coupling on current detection can be reduced by proper shield setup and optimization, which is applicable in both conventional wire-wound and PCB-type Rogowski coils.

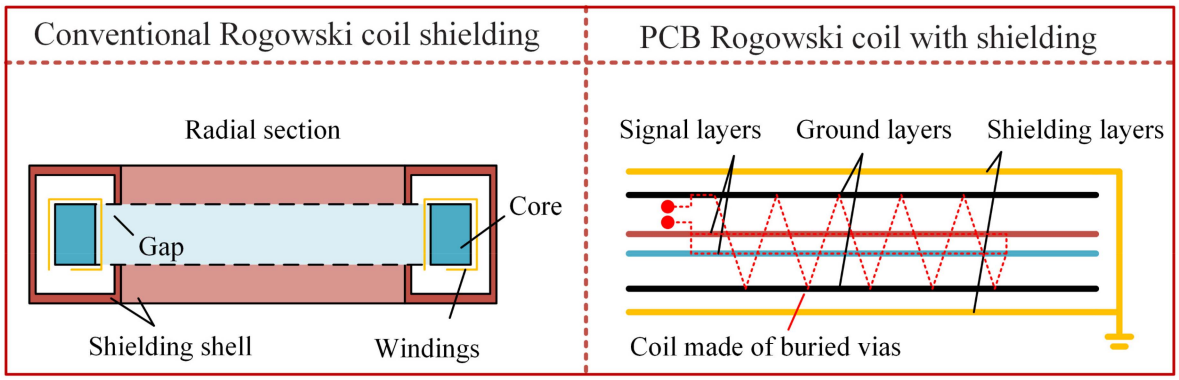

FIGURE 8. **Structures of conventional wire-wound and PCB Rogowski coils with shielding [41].**

D. SUMMARY

Rogowski coils are widely used in high-current measurements in power systems due to their advantages, such as high linearity, high stability, no saturation, small size, and safety due to an open circuit on the secondary side. These devices include fault high-current sensors for the protection of high-voltage power cables, capacitor banks, and power transformers [66]; ns/kA-level high-impulse current sensors related to short circuits and insulation testing in high-voltage ac high-capacity power system equipment [67]; and lightning current measurement sensors in communication towers and wind turbines [68]. These coils are also used in transmission line detection [69], current monitoring and sensing in smart substations [70], differential protection of hot stove transformers [71], pre- and postarc current measurements in circuit breakers [72], and local discharge detection [73]. In addition, Rogowski coils outperform conventional current transformers in power system metering and protection, as exemplified above, and excel in measurements of steady-state ac, fault transient currents, and large impulse currents, with advantages over current transformers, such as good large-load tolerance, wide saturation-free bandwidth, good transient response, ability to measure large currents, and low cost.

Despite the great potential of Rogowski coils, three challenges need to be addressed. The first is the difficulty of detecting dc or low-frequency currents, a limitation caused by the measurement principle of Rogowski coils. One possible solution is a hybrid measurement method, such as integrating a Hall sensor or magnetostrictive sensor with a Rogowski coil on a microchip, thus enabling effective simultaneous measurement of dc and low-frequency currents [74]. However, this method has difficulty measuring large currents and cannot be effectively shielded; perhaps laying an array of Hall sensors on a PCB Rogowski coil can solve the above problem. The second problem is the difficulty of accurately modeling Rogowski coils, which is because of the complex and diverse structure of the coils and because PCB-type Rogowski coils are rectangular rather than round, as is commonly assumed in theoretical calculations. These issues complicate the general modeling of Rogowski coils and increase the practical testing burden. Perhaps a combined field and path approach based on finite element simulation, supplemented by the parameter prediction capability of machine learning, could solve the above problems. Finally, there is the difficulty of achieving interference immunity of Rogowski coils at high frequencies. The existing methods for weakening electromagnetic interference with far-field radiation and near-field coupling were reviewed earlier, and they all introduce large parasitic inductances or capacitances for the entire Rogowski coil. This leads to a smaller resonant frequency and makes it difficult to achieve accurate measurement of high-frequency currents. Therefore, more effective anti-interference techniques must be proposed, or an optimal compromise between shielding and bandwidth needs to be found. Until these problems are solved, additional research is needed on Rogowski coils as an essential electronic component in power systems.

IV. FIBER OPTIC CURRENT SENSING

With the continuous transformation of the traditional power grid to a new generation of smart grids, the power system has gradually placed higher requirements on high-sensitivity monitoring of currents, effective distribution of electrical energy, and development of miniature relay protection devices. Although traditional current transformers are among the most widely used and vital online monitoring instruments in modern power systems, they have problems, including large size, complex insulation structure, flammability and explosion, and poor accuracy in the context of high-voltage and large-capacity power transmission. Furthermore, compared with current transformers, Rogowski coils have advantages for measurement of steady-state ac currents, fault transient currents, and large impulse currents. However, this method also has problems in terms of dc detection, accurate modeling, and interference resistance. Therefore, to solve these problems, there is an urgent need to investigate new current transformers to meet the new needs of smart grids.

As an essential means of reform and development of the global power grid, optical fiber sensing technology has unique advantages in the automatic monitoring and control of power systems, enabling the rational allocation of electrical energy

TABLE 3 Comparison of Fiber Optic Sensor Performance

Method	Amplitude (kA)	Frequency (kHz)	Cost	Disadvantages	Advantages
Photoelectric hybrid [78],[79], [80],[81],[82]	1000	10000	Medium	A transitional solution with high cost	Good insulation performance, strong resistance to electromagnetic interference, high safety, small size
Faraday magneto-optical all-fiber – Sagnac [83],[84],[85]	500	1000	Low	Low sensitivity, sensitive to environment, poor long-term stability	Anti-electromagnetic interference, wide measurement dynamic range, low power consumption, low cost and insulation
Faraday magneto-optical-all-fiber reflective [86, 87]	500	1000	Low	Low sensitivity, sensitive to environment, poor long-term stability	Resistant to electromagnetic interference, wide measurement dynamic range and high accuracy, low power consumption, low cost and insulation
Faraday magneto-optical-block glass [94],[95],[96],[97],[98],[99]	720	34	Low	High processing difficulty, fragile	Higher reliability, smaller size, virtually unaffected by linear birefringence
Magnetostriction – fiber optic interferometric [100],[101],[102]	0.01	0.05	High	Immature technology, high cost, high environmental impact	Interference-resistant, multiphysics measurable, unaffected by linear birefringence
Magnetostriction – fiber grating type [103],[104],[105],[106],[107],[108]	1.2	0.05	High	Poor stability and reliability, high cost, high environmental impact	High precision, fast response time, wide range, high sensitivity
Thermal effect micro/nano fiber [109],[110],[111],[112],[113]	0.12	0.5	Medium	Contact type, easily affected by the environment	High precision, good linearity

resources and ensuring the safe, reliable, and high-quality transmission of electrical energy. Since the first optical current sensor was proposed in 1963, many scholars worldwide have conducted considerable research on its principle, design, and technology, which have been practically applied in the fields of aerospace, rail transportation, and national defense security. The British Electric Power Company successfully developed an all-fiber optic current sensor (AFOCS) in 1977, followed by related research in Japan and the USA; China developed a fiber optic current sensor in 1989 at the Shenyang Transformer Factory and Tsinghua University, and it was practically applied in Siping city, Jilin Province [75], [76]. Compared with traditional current transformers, fiber optic sensing technology has the advantages of a wide dynamic range, good corrosion resistance, simple insulation structure, high measurement sensitivity, easy installation and maintenance, low cost, small size, high safety factor, and wavelength division multiplexing characteristics, which can meet the development needs of modern smart grids [77]. Depending on the operating principle, fiber optic current sensors can be classified into the following four categories: photoelectric hybrids, Faraday magneto-optical devices, magnetostrictive devices, and thermal effect devices. In this section, the principles, key technologies, and development status of fiber optic current sensors are summarized and reviewed in the above four categories, and the performance comparison of different types of fiber optic sensors is shown in Table 3. Possible solutions to their many problems and challenges are given.

A. PHOTOELECTRIC HYBRID TYPE

The photoelectric hybrid active current transformer is a new type of electronic current transformer based on traditional current sensing and optical fiber transmission technology and uses active device modulation technology, as shown in Fig. 9. This photoelectric hybrid transformer consists of a sensing probe, a data acquisition unit, a signal transmission system, and a power supply system. The transformer first uses an electromagnetic transformer, a shunt, or a Rogowski coil to collect the current signal from the line under test, then transmits the optical signal after electro-optical conversion to the low-voltage side through the optical fiber, and finally sends the low-voltage electrical signal to the signal processing end through photoelectric conversion. This active-type photoelectric transformer needs a working power supply and has a relatively simple structure and high reliability and accuracy. The photoelectric hybrid transformer based on Rogowski coils has the advantages of both Rogowski coils and optical fibers, i.e., a wide range, no magnetic saturation, good linearity, and better insulation performance, which reduce the cost of sensor processing and manufacturing and avoid the complexity of the optical path and structure of passive-type transformers.

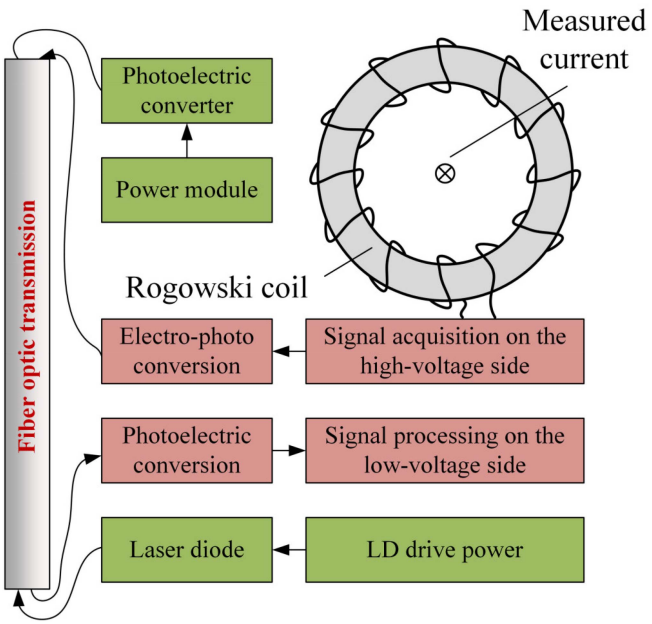

FIGURE 9. **Schematic diagram of a hybrid photoelectric current transformer based on a Rogowski coil [78].**

However, this method requires special signal processing circuits on the high-voltage side, which are greatly dependent on a stable power supply system.

Photoelectric hybrid current transformers have been studied for many years. A photoelectric hybrid sensor suitable for high-voltage power systems was proposed by Pilling et al. [78], and theoretical and experimental studies were conducted. However, the measurement accuracy of this sensor is related to the environmental variables represented by temperature, and the signal-to-noise ratio is low, making it challenging to measure larger currents. To solve these problems, Dull et al. [79], proposed an optoelectronic hybrid current sensor for accurate metering and relay protection of large currents and combined a Rogowski coil with a passive integrator, which showed good linearity at both A–kA levels. The maximum value of the sensor's ratio error was 0.3% in a temperature cycling test of −30 °C to 70 °C [79]. However, this sensor still suffers from temperature drift. Xie et al. [80] developed an optical digital local control and measurement system to control and monitor the status of switches, relays, and thyristors and used an optoelectronic hybrid current transformer to measure the discharge current and voltage of a capacitor bank. The results showed that the system achieved 99% accuracy and could measure large currents up to 20 kA [80]. However, the system is complex, expensive, and large, so it cannot be used in current detection schemes based on small sensors. To address this challenge, Orr et al. [81] proposed a new sensor that combines fiber Bragg gratings and Rogowski coils and used this sensor in relay protection current measurements to achieve serial multiplexing of optical fibers with the advantages of a wide dynamic range, small size, and weak interference. However, studies have shown that the measurement accuracy of such small sensors is relatively low, and temperature drift is evident, so meeting the demand for high-precision detection is challenging. To address these issues, Wei et al. [82] combined a Rogowski coil with a reflector-based MEMS device in a high-voltage environment to design a small optoelectronic hybrid current sensor and tested the steady state, transient, frequency, and temperature response of the sensor. The test results showed that the sensor's error drift was only 0.5% and 1% in a current range of 20–480 A and temperature range of −20 °C to 80 °C, respectively, and cost-effective and low-power current sensing were achieved.

As seen from the above study, the optical fiber in this type of photoelectric hybrid current transformer functions only as a transmission medium and exploits the many advantages of the Rogowski coil to improve the dynamic response of the sensor. The optical fiber in this sensor is an insulating material, which helps solve the problem of high-voltage isolation; the transformer does not fail due to core flux saturation and can measure a relatively wide dynamic range of current. In addition, the output of this transformer is an optical signal, which avoids electromagnetic interference and does not present the risk of a high-voltage open circuit on the secondary side; thus, this transformer has the advantages of good insulation performance, strong anti-electromagnetic interference, high safety, and small size. However, this sensor does not fully exploit the advantages of optical fibers; rather, it functions only as a transitional solution used in current measurements. Therefore, the sensing and signal transmission components are optical fibers, and optical devices with current sensors will be an important future development direction for this technology.

B. FARADAY MAGNETO-OPTICAL TYPE

1) ALL-FIBER

An AFOCS is a type of Faraday magneto-optical sensor that mainly uses an optical fiber as the sensing element and signal carrier to obtain information about the measured current. The basic principle of the AFOCS is that the magnetic field generated by the measured current changes the transmission time of the left and right circularly polarized light in the optical fiber, thus enabling the measurement of current through the resulting nonreciprocal phase difference. In terms of the optical path structure and signal detection method, AFOCSs can be divided into two categories, as shown in Fig. 10: polarization-type AFOCSs, which directly detect the Faraday rotation angle of the output optical signal, and interference-type AFOCSs, which use a phase modulator to detect the phase difference of the output optical signal.

Fig. 10(a) shows the basic structure of the polarization-type AFOCS, which reveals that the light from the light source reaches the fiber ring after passing through the delay coil and the polarizer and that the output linearly polarized light enters the signal processing module through the delay coil and the polarizer, thus achieving single-optical-path detection [83].

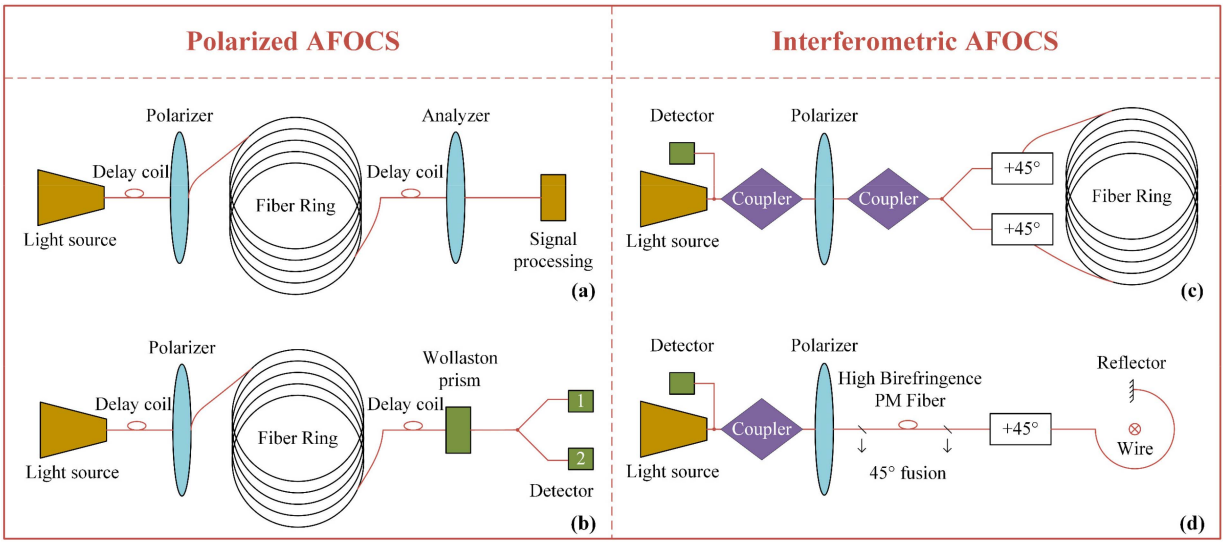

FIGURE 10. **Different structures of AFOCSs. (a) Single-optical-polarization AFOCS. (b) Dual-optical-polarization AFOCS. (c) Sagnac interferometric AFOCS. (d) Reflective interferometric AFOCS [83].**

This structure is easier to implement but cannot be used to measure dc currents. To solve this problem, Papp and Harms [84] proposed a dual-optical path detection scheme based on Wollaston prisms, which enables temperature compensation while also enabling dc measurements. As shown in Fig. 10(b), this dual-optical-path polarization-type AFOCS resolves the two orthogonally polarized light beams emitted from the Wollaston prism separately, including the relationship between the light intensity and Faraday rotation angle. The experimental results show that the dual-optical path structure is more sensitive to the external environment, although the measurement sensitivity is somewhat improved. Therefore, using a costly low-birefringence fiber as the sensing fiber for AFOCSs is a feasible solution.

In contrast to the detection principle of polarization-type AFOCSs, interference-type AFOCSs use a phase modulator to detect phase changes in optical signals to obtain measured current information; these types of AFOCSs can be divided into two types, Sagnac and reflection, according to their structures. Fig. 10(c) shows the schematic structure of the Sagnac-type AFOCS, where the light signal emitted by the light source is converted to linearly polarized light by the coupler and the starter. Subsequently, the coupler is divided into two signals and converted into circularly polarized light, which enters the fiber ring in opposite directions and emits an optical signal with current information. The emitted light is then reversed through the whole structure, interfered with at the polarizer, and received by the detector [85]. As shown in the figure, this structure requires high processing and fabrication costs due to the application of two $\lambda/4$ waveplates, and its sensitivity is much lower than that of polarized AFOCSs.

Another interferometric AFOCS has a reflective structure, as shown in Fig. 10(d), which includes both an orthogonal conjugate reflector and a Faraday rotation mirror [86]. Unlike in the Sagnac type, linearly polarized light is divided into two mutually perpendicularly polarized beams at the 45° fusion point, and then, the left and right circularly polarized light is injected into the fiber ring by the $\lambda/4$ wavepiece. After reflection and interference at its end, the optical signal containing the current information is output through the detector. The reciprocal rotational light is canceled by this structure, thus significantly reducing the influence of environmental factors. Moreover, this reflective structure is less dependent on optics and has higher sensitivity and reliability than other AFOCSs. It should be noted, however, that ordinary phase modulators have difficulty achieving simultaneous biaxial modulation of left and right circularly polarized light, thus limiting the quality of the output signal of this structure [87].

Although the development of the AFOCS has continued for more than 50 years, the method has not been used on a large scale in engineering practice because of problems, such as low detection sensitivity due to temperature sensitivity, poor detection stability due to linear birefringence, and the lack of adequate data processing algorithms. Among temperature compensation methods, He et al. [88] proposed a temperature-controlled circuit for semiconductor lasers to obtain a relatively constant temperature and constant flow of the light source, and the measurements showed that the standard deviation of the output wavelength could reach 10^{-7} orders of magnitude. Alternatively, Yang et al. [89] used a novel fiber delay coil with an insulated cavity to compensate for temperature variation errors and used it in fiber optic gyroscopes and current sensing. Hu et al. [90] focused on the temperature compensation method for $\lambda/4$ wavelets. These scholars used a $\lambda/4$ waveplate with a negative temperature coefficient to compensate for the positive changes in the Fielder constant, resulting in an output error of less than 0.2% in the range of -40 °C to 85 °C [90]. In the linear birefringence suppression method,

new special fibers, such as twisted, highly refractive fibers and polygonal polarization-preserving photonic crystal fibers [91], can effectively suppress the linear birefringence effect caused by nonidealized bending and external squeezing. However, the high cost of special optical fibers limits the widespread use of this approach. Another method for suppressing linear birefringence is improving the sensing head structure by using different winding methods and reflector position adjustment to increase the sensitivity of the AFOCS in current detection. Finally, in the study of data processing algorithms, the application of artificial intelligence-based nonlinear temperature correction methods and second-harmonic error complementation algorithms can significantly reduce the current measurement error, and the adoption of additional new algorithms has great potential for improving detection sensitivity and reliability.

In conclusion, AFOCSs have been widely studied for high-voltage and high-current detection in power systems, and scholars have continuously used many means to improve the sensitivity and reliability of AFOCSs. These improvements include a new AFOCS based on a single-polarization single-mode coupler and fiber ring structure [92], an AFOCS based on an optical switch and ring cavity structure, an AFOCS using an integrated-optic polarization splitter combined with a reflective AFOCS [93], and an AFOCS with coupled Faraday rotators. However, although the stability of the sensors has improved, the effects of environmental changes, such as temperature, vibration, electromagnetic interference, and optical interference, have not been eliminated. Therefore, an important direction for future AFOCS development is to achieve environmentally adaptive measurement, including the use of wavelength division multiplexing technology to measure different locations of a variable through the same structure and intelligent compensation algorithms for multiple environmental parameters. Furthermore, the combination of intelligent cloud platforms and edge computing technologies has the potential to transform AFOCSs from smart grid to transparent grid applications.

2) MAGNETO-OPTICAL GLASS CURRENT SENSOR

Compared with AFOCSs, magneto-optical glass current sensors tend to be more reliable, smaller in size, and virtually unaffected by linear birefringence and operation, as shown in Fig. 11. In 1973, Rogers [94] designed an optical glass current transformer intended to be inexpensive, accurate, and robust and analyzed its structural parameters and environmental robustness. In general, this type of sensor uses magneto-optical glass with a large Verdet constant as the sensing element and indirectly measures the current by measuring the Faraday rotation angle of the output linearly polarized light [95]. According to the ion doping species, the Verdet constants of paramagnetic glasses, represented by rare earth glasses, are much greater than those of inverse magnetic glasses, such as flint glasses, which are widely used today. Although current sensors based on the latter are less sensitive, they are almost

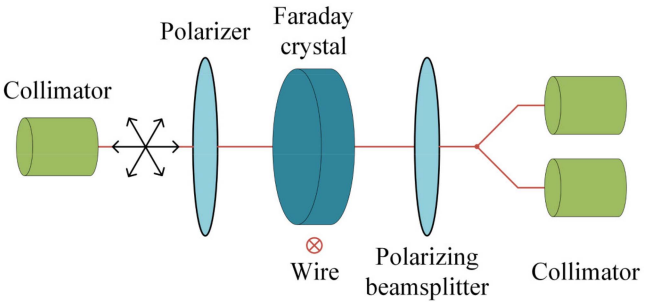

FIGURE 11. Schematic diagram of the operating principle of the magneto-optical-glass current sensor [94].

independent of temperature and are more reliable. However, the reflection structure of the sensing head of a magneto-optical-glass current sensor is very complex, so a reflection phase shift is easily introduced during the reflection process. This turns the two orthogonal linearly polarized light beams into elliptically polarized light and reduces the measurement accuracy.

To solve the above problem, Sato et al. [96] proposed a double orthogonal reflection scheme to weaken the interference of the reflection phase shift, i.e., using two reflections instead of the original one. The two light components exhibit a phase difference of 90°, thus offsetting the phase shift of the two reflections. Although this method has high stability and accuracy with respect to long-term monitoring, the effect of temperature variations has not been addressed. However, Maffetone and McClelland [97] tested the vibrational and temperature stability of optical glass current sensors with lightweight polymer fibers from the viewpoint of temperature compensation. Nevertheless, these sensors are still expensive and difficult to use in large numbers [97]. Niewczas et al. [98] used FR5 crystals as a sensing head to improve magneto-optical glass materials. These scholars found that the measurement error of this sensor was only 0.2% when the ambient temperature varied from −45 °C to 140 °C.

Moreover, the distortion of the signal waveform caused by mechanical vibration was reduced by 30 dB at a frequency of 5 kHz, and the measurement accuracy was significantly improved. In another study, targeting the sensing head structure, Wang et al. [99] used ring-shaped retarded refractive index magneto-optical glass to avoid a reflection phase shift. While ensuring a uniform refractive index at the center of the glass, the inner and outer layers of this magneto-optical glass have a variable refractive index, which prevents the light beam from reaching the interface between the glass and air. In summary, because of their small size and simple structure, optical glass current sensors are used more often in relay protection and current monitoring. However, the sensitivity of such sensors can be affected by many environmental factors, such as temperature, vibration, external magnetic field, and current, so a high current detection accuracy is difficult to obtain. Therefore, leading future research directions in this area include the development of new low-cost magneto-optical glass current

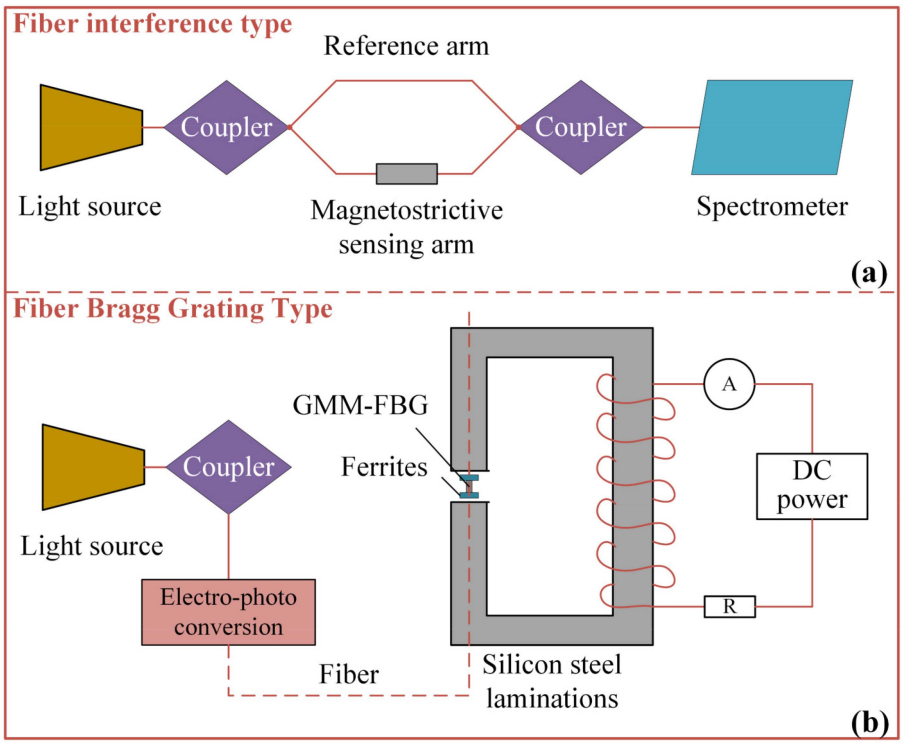

FIGURE 12. Current sensor based on the magnetostrictive effect. (a) Fiber optic interferometric type. (b) Fiber grating type [100].

sensors with high accuracy, long-term stability, no reflection phase shift, and no temperature drift.

C. MAGNETOSTRICTIVE TYPE

Magnetostrictive sensors utilize the magnetostrictive effect. That is, the strain of the material as a function of the magnetic field can be used to determine the current parameters. These sensors can be classified into two types: the interference type and fiber grating type. The principle of fiber-optic interferometric current sensors is that the sensing arm coated with a magnetostrictive material is strained as the amplitude of the measured current changes, resulting in a change in the output spectrum, thus enabling effective measurement of the current, as shown in Fig. 12(a). In the fiber optic current sensors of interferometers, including Mach–Zehnder, Michelson, and Sagnac interferometers, magnetostrictive materials are applied to the different interferometric sensing arms. The two-optical-path system of the first two interferometric structures greatly impacts the measurement accuracy. To solve this problem, Fisher et al. [100] attached optical fibers to piezoelectric ceramics and used an F-Z interferometer for dynamic demodulation, effectively improving the current measurement accuracy. Wang et al. [101] designed an H-type weak dc measurement sensor with an excellent linear response based on the principle of the fiber-optic weak electric field sensor of a Michelson interferometer; this sensor demonstrated good stability, high sensitivity, and good linearity. However, in this article, the degree of influence of environmental factors on the sensor was not analyzed. Despite the high detection accuracy and fast response of interferometric magnetostrictive current sensors, the sensor performance is closely related to the output stability of the light source because it detects the light intensity and the stability and reliability of the optical fiber itself. It is also susceptible to external environmental changes. Therefore, ensuring the robustness of interferometric magnetostrictive current sensors is generally difficult [102].

Compared with interferometric sensors, the fiber grating-based approach is more widely used, and its principle is shown in Fig. 12(b) [103]. The giant magnetostrictive material (GMM) deforms with a change in the magnetic field generated by the measured current; this causes a strain in the fiber grating and a drift in the wavelength of the reflected light. Finally, information about the measured current is extracted by a demodulation device. Based on the working principle of the GMM fiber grating current sensor, there is a cross-sensitivity problem of temperature and strain in the fiber grating. The GMM generates an increase in temperature due to its internal ferromagnetic loss, which reduces the sensor's measurement performance and makes the output optical signal more complex and difficult to distinguish. Therefore, many scholars have thoroughly studied the temperature compensation and signal demodulation of GMM fiber grating sensors. To address the former problem, Reilly et al. [104] placed a GMM fiber sensor in a solenoid, used an F-P tunable filter for ac detection, and performed temperature drift tests in the range of 18 °C–100 °C. However, the nonlinearity and phase hysteresis problems under high-current measurements have

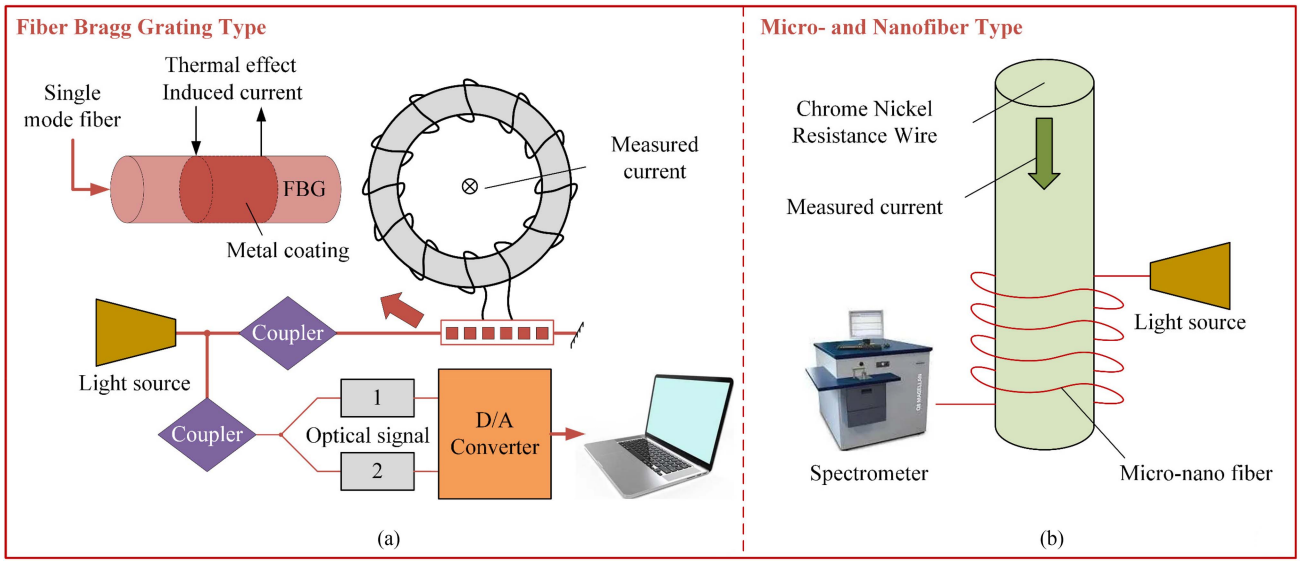

FIGURE 13. **Thermal effect type fiber optic current sensor. (a) Fiber grating type [109]. (b) Micro- and nanofiber type [113].**

not been properly addressed. Han et al. [105] suppressed the temperature-induced common-mode signal based on a dual-fiber grating structure to weaken the temperature effect on the current sensor's detection sensitivity, but the method was validated only in the narrow temperature range of 20 °C–70 °C with a large sensor. In the design of small sensors, Jiang [106] proposed a temperature compensation method for GMM fiber grating current sensors based on field-programmable gate array (FPGA) chips. These researchers used a complex combined system of temperature sensors, a temperature control circuit, and a laser driver circuit to achieve temperature drift suppression by automatically adjusting the control voltage of the DSP of the demodulation system with the FPGA. To address the signal demodulation problem, Chiang et al. [107] applied a fiber grating to two different fiber structures and used inexpensive optical intensity demodulation to achieve simultaneous ac and dc measurement; these structures demonstrated advantages, such as compactness, affordability, and multiplexing. Mora et al. [108] applied Terfenol-D rods and optical fibers to a power line. They used the 50 Hz and higher harmonic components as current sensing information and the zero-frequency component of the dynamically demodulated output signal of the optical fiber as temperature information to achieve effective joint measurement of the wavelength-encoded temperature and amplitude-encoded current.

Compared with other types of fiber optic sensors, GMM fiber grating current sensors have more obvious advantages, such as interference resistance, measurable multiphysics, and easy wavelength division multiplexing, and are not affected by linear birefringence. However, the impact of ambient temperature on detection accuracy is still large, and optical signal demodulation equipment is complex and costly. Therefore, there is an urgent need for a highly reliable temperature compensation method and a high-precision and low-cost demodulation method that can integrate the advantages of GMM fiber grating current sensing technology to achieve reliable monitoring of high currents in power systems. At present, because of the demand for distributed cloud monitoring in transparent power grids, combining multiple fiber optic sensors with communication system multiplexing technology to construct a miniaturized optical current sensing network may be a frontier area of research for future GMM fiber grating current sensor development.

D. THERMAL EFFECT TYPE

Thermal effect optical current sensors exploit the temperature-dependent phenomenon of the material refractive index to obtain information about the current by measuring the Joule heat generated by the current flowing through a conductor. These current sensors can be divided into fiber grating and micro/nanofiber (MNF) sensors, depending on the fiber material. In the former, a thermistor and an optical fiber are directly glued together, as shown in Fig. 13(a), and the heat generated by the current flowing through the thermistor is used to change the refractive index of the optical fiber, thus changing the output of the optical system. Cavaleiro et al. [109] used a method of laying down metal films similar to thermistors. The heat generated by the current flowing through the metal film can deform the film; thus, the wavelength of the center of the reflection spectrum of the fiber grating changes, which corresponds to a change in the current. After experimental verification, it was determined that this sensor can accurately and repeatedly measure current. However, the uniform plating process of the metal film is more complicated than that of other materials, and the sensitivity and response delay of the sensor are affected by the uniformity of the metal film. In addition, the external ambient temperature can impact the

central wavelength of the fiber grating, and there is a lack of effective solutions.

With its advantages of small size, high sensitivity, and low environmental impact, in recent years, MNF technology has gradually emerged, and different types of thermal effect MNF current sensors have been proposed; their basic principles are shown in Fig. 13(b). The thermistor is wound from an MNF, and the magnitude of the current flowing in the thermistor changes the resonant wavelength of the MNF, which has been verified to be linearly related to the square of the current [110]. Belal et al. [111] used the heat generated as current passed through a copper wire coated with a very thin Teflon film to create a phase drift in an MNF and to measure the ac current at frequencies below 500 Hz. These scholars found that the response characteristics of the sensor could be improved by reducing the diameter of the copper wire or by using a higher resistivity MNF material. Yan et al. [112] used a metal rod coated with a single-layer graphene film as an optical fiber winding object. These researchers used the thermo-optical and thermal expansion effects of the graphene film to change the resonant wavelength of the microfiber coil resonator to achieve a current detection sensitivity of 67.297 μm/A^2. However, this method requires a tradeoff between reducing the resistance of the graphene sheet and increasing the current measurement sensitivity in practical applications. Sulaiman et al. [113] used the resonant wavelength shift characteristics of the Mach–Zehnder MNF structure at different temperatures to measure the current. The experimental results showed that the measurement sensitivity varied from 0.32 to 0.54 nm/A^2 for different copper wire and fiber contact areas.

Based on the abovementioned studies, to further improve the sensitivity of MNF current detection, a Mach–Zehnder MNF interferometer was proposed by Jasim et al. [114]. This instrument uses Joule heat generated by dc currents to change the refractive index of the MNF to produce a phase difference between the two arms of the interferometer, and the correlation coefficient and measurement sensitivity reached 0.99 and 140.26 pm/A^2, respectively. These thermal effect-based fiber optic current sensors are generally small and have a relatively simple implementation principle, and their detection sensitivity can easily reach a high level. Current sensors with MNF structures are more suitable for compact applications and have advantages in integrating optical current sensing systems. However, such MNFs are prone to contamination and corrosion in the air, are less reliable and more expensive than other materials, and are often very limited in practical use. Therefore, future research should involve researching MNF materials with better reliability, reducing their manufacturing and processing costs, or continuously optimizing their structural parameters during current measurement.

E. SUMMARY

Fiber optic current sensors are widely used in the current monitoring of lines, power plants, substations, small equipment, and cables in smart grids due to their resistance to interference, extensive range, high accuracy, low power consumption, low cost, good insulation performance, long transmission distance, and other advantages. These devices include initial transitional optical current sensors based on a mixture of Rogowski coils and optical fibers, subsequent Faraday magneto-optical pure optical current sensors with smaller sizes and better temperature stability, and strain-gauge optical current sensors with higher stability and response speed using magnetostriction and thermal effects as auxiliary sensing methods.

Despite the great potential of fiber optic current sensors, in modern intelligent power system condition monitoring, these sensors suffer from linear birefringence, temperature drift, vibration sensitivity, and other problems. Their failure rate is more than ten times that of traditional electromagnetic transformers, which is unfavorable for power grid operation, maintenance, and repair [115]. To address the above problems, a spiral structure with Hi-Bi fibers has been proposed and effectively solves the linear birefringence problem. Second, research on waveplate temperature self-compensation technology reduces the measurement error of fiber optic current sensors with temperature drift. For sensors that are sensitive to vibration, the proposed optical multiplexing technology and various damping methods can effectively improve the vibration resistance of fiber optic current sensors. However, the impact of environmental changes on fiber optic current sensors cannot be eliminated, and new sensor structures need to be designed to minimize or eliminate this impact in the future; these include simple optical circuit designs with fewer devices, more stringent device selection criteria, and intelligent processing of optical signals with environmental adaptation.

V. CURRENT SENSING USING MAGNETIC FIELD MEASUREMENTS

As smart grids evolve with an increasing number of connected smart devices and renewable energy sources like wind, tidal, and solar power, they require advanced, intelligent control to manage the unpredictability of power output from these sources. Critical to this control is the accurate and reliable current sensing in grid monitoring. While shunts are favored for their simplicity and accuracy, Rogowski coils are noted for their effective current measurement without saturation and high safety. Fiber optic sensors are also prevalent in smart grids for their numerous benefits, despite their challenges like size and integration complexity. With the shift toward comprehensive state sensing in transparent power grids, research is advancing in high-current sensing technologies that offer noncontact measurement, high isolation, and environmental suitability, aligning with the integration demands for intelligent sensing and control systems in smart grids.

In this section, based on different measurement theories, high-current sensing technologies based on magnetic field measurements are classified into four categories, namely, Hall sensing, magnetoresistive sensing (including anisotropic magneto resistance, AMR; giant magneto resistance, GMR; and tunnel magneto resistance, TMR), MEMS-based ME sensing

TABLE 4 **Comparison of the Performance of Magnetic Field Current Sensors**

Method	Amplitude (kA)	Frequency (kHz)	Cost	Disadvantages	Advantages
Hall sensor [116],[117],[118],[119], [120],[121],[122],[123], [124],[125],[126]	100	1000	Low	Low sensitivity, sensitive to environment, narrow frequency measurement rate range	Extensive application range; good linearity; can measure DC, AC, and pulse current
AMR [128],[129], [130]	1×10^{-6}–1.6	10000	Low	Narrow linearity range, easy magnetic saturation	Good linearity, small size, simple process, low cost
GMR [131],[132], [133],[134]	1.6	10000	Medium	High production cost	Small size, high sensitivity, wide measurement range
TMR [135],[136],[137],[138], [139],[140],[141],[142]	2×10^{-8}–10	10000	High	Complex manufacturing process	High-temperature stability, high sensitivity, wide linear range
ME [144],[145],[146], [147],[148],[149]	1×10^{-11}–1.2	5×10^{-6}–200	Low	Slow theoretical development, less research on high current detection	Passive, small size, high sensitivity
SAW [150,[151],[152], [153],[154][155], [56],[157],[158, [159],[160,[161], [162],[163]	0.01–0.8	0	Low	Research is only available for DC magnetic field/current measurement	A lower detection limit of 0.05 mA

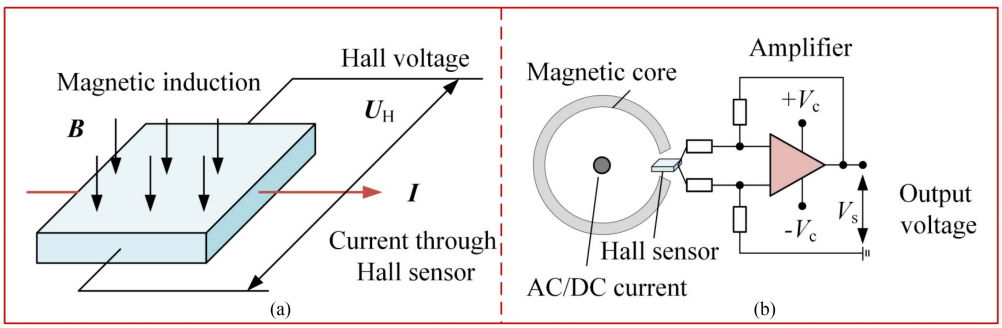

FIGURE 14. **Schematic diagrams of the structure of a Hall sensor: (a) hall current sensing principle and (b) a hall sensor measuring current [116].**

and SAW sensing methods, as shown in Table 4. The development status of these methods and possible future development directions are reviewed.

A. HALL SENSING

In the presence of an applied magnetic field, the current flowing through a Hall element is converted into an electric voltage proportional to the input current, and a device that uses this Hall effect to measure the input current is called a Hall sensor. This sensor has the advantages of high isolation and good linearity, and its principle is shown in Fig. 14. Fig. 14(a) shows that applying a magnetic field in the direction normal to the energized wire causes a Hall voltage $U_H = R_H IB/d$ at both ends of the energized wire. Here, R_H is the Hall coefficient, I is the current, B is the magnetic induction, and d is the thickness of the Hall element. The above equation shows a linear relationship between the magnetic induction intensity B and the magnetic induction potential R_H in the Hall element, which is one of the advantages of Hall sensors. Fig. 14(b) shows a schematic diagram of the Hall sensing current measurement; a wire crosses the magnetic core, and a Hall sensor is placed in the air gap. The magnetic field generated by the measured current is concentrated at the air gap, and the Hall voltage is induced in the Hall element. An op amp circuit amplifies this voltage, and a voltage signal proportional to the measured current can be obtained, thus providing information about the measured current.

Early Hall-sensing current measurement methods demonstrate poor linearity, low sensitivity, environmental sensitivity,

and a narrow frequency measurement range, thus limiting the application of Hall sensors. To solve the problem of the poor linearity of current measurements due to the nonuniformity of magnetic materials, Waeckerlé et al. [116] designed an open-loop, high-precision dc Hall sensor. These researchers found that the measurement accuracy was related to the air gap accuracy and the nonlinearity of *B-H*, and an increase in the air gap could improve the uniformity of the magnetic field. However, the designed larger air gap tends to result in lower measurement sensitivity, reducing the current sensing accuracy. Consequently, scholars are exploring the enhancement of the magnetic field measurement sensitivity by minimizing the air gap as a potential solution to this problem. Popovic et al. [117] proposed a field concentrator-based magnetic field sensing method for small current measurements. This method was experimentally verified to have a nearly tenfold greater magnetic field resolution than the conventional method, achieving 99% accuracy in current measurements up to 12 A, and it can be applied to both PCB conductors and independent conductors for current measurements. However, such highly integrated sensors are susceptible to external environmental influences, such as temperature and magnetic field perturbations, and their reliability decreases during long-term use. Frick et al. [118] reported that a dual Hall sensor array can attenuate the effects of environmental changes, especially common mode noise from external magnetic fields, and that this method can achieve 99.5% accuracy when measuring 5 A currents. Measurement arrays composed of more Hall sensors were proposed by D'Antona et al. [119] and supported by signal processing techniques based on the resolution of multiphase current measurement principles; the arrays performed well for current measurements up to 20 kA. However, these sensor array-based methods can measure a narrow range of frequencies, and the measurement error is especially large at higher frequencies of the measured current. To solve this problem, Dalessandro et al. [120] combined a low-turn-count current transformer with a Hall element so that the two mutually covered the portion of the frequency that each could not measure, increasing the measurement frequency to 30 MHz while retaining the original advantages of Hall sensors. The abovementioned studies show that current measurement methods using Hall sensors either exhibit small and narrow frequency ranges or have complex structures that substantially increase the sensor processing costs.

Therefore, low-cost Hall sensors based on silicon complementary metal–oxide–semiconductor technology have been proposed and widely used, but such current sensors generally experience a large measurement bias and temperature drift. In magnetic field measurements, Mosser et al. [121] combined the GaAs quantum well Hall effect technique with the spinning current modulation technique to enable the measurement of weak magnetic fields of 30 nT. In another study, Crescentini et al. [122] proposed an integrated Hall sensor and used it for current measurements in power converters in power electronics devices. These investigators also used the spinning current modulation technique and measured the current using a very small differential amplifier, which has a low offset of 350 μT and a high measurement frequency of 1 MHz. Blagojevic et al. [123] reviewed the progress of Hall sensors with a Sentron CSA-1 and a built-in magnetic concentrator, which can measure ac and dc from tens of milliamps to hundreds of amperes. These proposed methods significantly reduce the production cost of Hall current sensors while increasing the measurement sensitivity and bandwidth. In recent years, flexible and differential Hall sensor arrays have been proposed by Zapf et al. [124] and George and Gopalakrishna [125], among others, and the range of sensor applications has greatly increased. It is clear that different types of current measurement methods based on Hall sensors are being optimized and proposed, and the amplitude and frequency range, accuracy, sensitivity, and reliability of the currents that can be measured have been improving, with increasingly high application performance. Currently, the use of magnetic field concentrators to increase the magnetic field strength and suppress external magnetic field interference is effective and widely used for improving the magnetic field sensitivity of Hall elements. However, additional cores introduce additional hysteresis and eddy current losses, which reduce the bandwidth and response speed of Hall sensors [126]. Closed-loop Hall sensors may be a solution for improving the nonlinearity of the core utilizing an external coil, but new problems arise; namely, the increased size and cost of the sensor make these sensors difficult to use in high-frequency, high-current measurement scenarios.

B. MAGNETORESISTIVE SENSING

With the increasing demand for miniaturized sensors with high sensitivity and low power consumption in transparent power grids, innovations in integrated current sensing elements are constantly being introduced. The Hall sensor introduced in the previous section is one of the most widely used and developed current sensing elements because of its simple implementation principle and low price. However, to increase the measurement sensitivity, the device size of Hall sensors should be scaled down. In addition, the high operating power consumption and bad SNR of these Hall sensors make it difficult for them to meet current sensing needs. In contrast, compared with Hall sensors, magnetoresistive sensors have the advantages of lower power consumption, higher sensitivity, easier integration, and good temperature drift characteristics, and they stand out in the application and development of transparent power grids [127].

In the magnetoresistance effect, the probability of electron tunneling varies, as the direction of electron spin polarization of the ferromagnetic material is related to the applied magnetic field, which affects the resistance of the magnetoresistor. The structure of a typical AMR is shown in Fig. 15(a); it is composed of a ferromagnetic thin-film material whose resistance is inversely related to the internal magnetization vector and the angle of the current. Zhenhong et al. [128] proposed an AMR sensor with an applied bias magnet, which has good linearity and small hysteresis and can measure currents up to

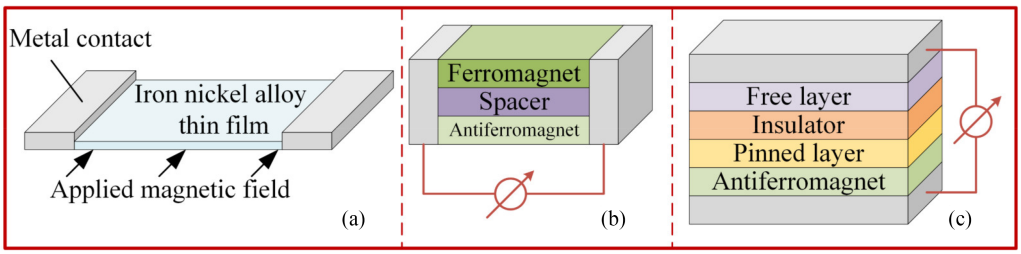

FIGURE 15. **Schematic diagram of magnetoresistive sensor structures with different principles. (a) AMR. (b) GMR. (c) TMR.**

300 A. However, this sensor is affected by temperature and has poor reliability. Mlejnek and Ripka [129] used an array AMR sensor to reduce the effects of environmental changes, but this sensor requires complex error compensation algorithms to support it. Regarding frequency characteristics, Nibir and Parkhideh [130] used planar magnetic concentrators to enhance the performance of AMRs in current measurements at high frequencies. These researchers experimentally showed that such AMRs could measure currents up to 400 kHz, which increases the measurement bandwidth by 33% compared with that of conventional AMRs, but the size of the sensor increases as a result. In general, although the sensitivity of AMR elements is much greater than that of Hall sensors, the linear range of AMRs is generally narrow and prone to magnetic saturation, so it is difficult to obtain a high signal-to-noise ratio and a low-temperature drift. The existing solutions to these problems usually increase the complexity of the component manufacturing process, and the power consumption and size of AMRs inevitably increase.

The GMR was developed based on the AMR, and its structure is shown schematically in Fig. 15(b). This structure is composed of two layers of ferromagnetic material sandwiched by a nonmagnetic metal film, and the magnitude of the magnetoresistance is related to electron spin-dependent scattering, a phenomenon discovered by Baibich et al. [131]. In their study, the GMR resistance variation at room temperature reached 12.8%, which is an extremely significant improvement compared with that of the 2% to 4% AMR, which has a smaller size and wider bandwidth. Using an artificial antiferromagnetic system, Vieth et al. [132] improved the linearity of the GMR by using two separate sensing chips with opposite response characteristics. This device performed well and had high sensitivity for current measurements up to 40 A. However, guaranteeing the consistency of this sensor between the two chips is difficult. Beltran et al. [133] processed a complete bridge with four GMR sensing elements simultaneously on a single chip, thus improving the temperature drift characteristics while ensuring the consistency of all the sensing elements. George and Gopalakrishna [134] used a GMR sensor model AA002-02 from NVE, USA, to measure the current; this sensor used a permanent-magnet bias method to achieve a high linearity range of up to 70 A in a magnetic field of 150 to 1050 μT, but the stability and reliability of the permanent-magnet bias were poor and needed to be further enhanced.

Compared to GMRs, TMRs were discovered much earlier [135], but it was not until 1995 that the tunneling magnetoresistance effect of these sensors at room temperature was reported [136]. Compared to AMR and GMR magnetic sensors, TMRs have higher sensitivity, lower power consumption and a satisfactory linear range, and they can achieve resistance changes of more than 230% [137]. The structure of these materials is shown in Fig. 15(c). The TMR uses an insulating layer to separate two ferromagnetic layers, where the upper layer is a free layer with a magnetization direction related to the applied magnetic field and the lower layer is a pinned layer with a constant magnetization direction. Electrons with fluctuations in the ferromagnetic layer can pass through the insulating layer with a certain probability and maintain the original spin direction; the greater the consistency of the magnetization direction between the free layer and the pinned layer is, the greater the probability of electron tunneling and the smaller the resistance of the TMR [138].

Yu et al. [139] used a circular TMR array to achieve noncontact measurements of ac and dc circuits and reduced the relative error due to wire position variations based on a theoretical analysis of the vector inner and outer products. These authors showed by calculation that the relative measurement error of the current is less than 0.2% in the position and angle offset ranges of 10 mm and 30°, but this finding has not been validated experimentally because these offsets cannot be measured in practice. Khawaja et al. [140] proposed a TMR sensing method with three Mu-metal arc shields to measure high currents in gas-insulated switchgears. These investigators determined that the response deviation of the sensor was only 0.83 for current measurements up to 1 kA, indicating good noise resistance and linearity. However, this method is limited to current measurements with fixed conductors and is less flexible. Zhang et al. [141] proposed a 3-D coreless TMR array current measurement and calibration method that does not require fixed conductor positions. This approach avoids the effect of the tilt angle between traditional 1-D sensor arrays and reduces the relative measurement error by nearly 18 times. However, the structure of these sensors is very complex, and the processing challenges are serious. Among the state-of-the-art studies, Li et al. [142] designed an array-type current

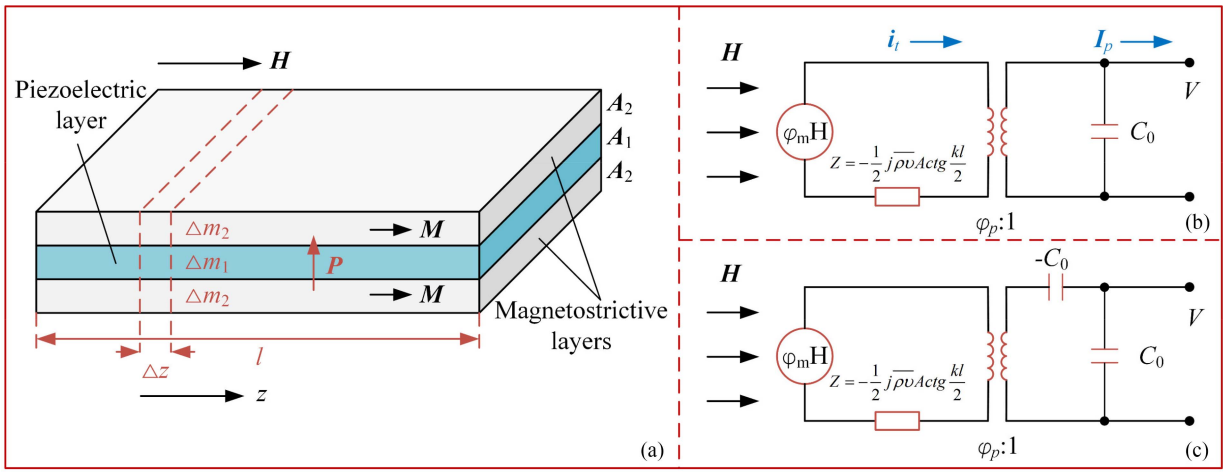

FIGURE 16. Schematic diagram of the structure of the ME sensor. (a) Principle of a ME material with a sandwich structure [143]. (b) Equivalent circuit model of an L-T mode ME composite [144]. (c) Equivalent circuit model of an L-L mode ME composite [144].

sensor with four TMR chips without enclosing conductors; the advantages of the simple structure, good robustness, lack of disconnected circuit installation, and low computational burden of the sensor in this study are better than those of the sensors in previous studies.

Current sensors based on magnetoresistive effects play a substantial role in solving the next generation of high-precision sensing problems. Compared with AMR and GMR sensors, TMR sensors offer significant advantages, including higher temperature stability and measurement sensitivity, a wider linear range, lower power consumption, and no need for additional pole magnetic rings or reset coil structures. Moreover, the performance of TMR current sensors continues to improve with further improvements in membrane material performance and further optimization of chip and circuit structures. Nevertheless, several technical challenges still need to be addressed, including the impact of low-frequency noise on the signal-to-noise ratio of the device and stability problems in 3-D magnetic field detection. Therefore, further optimization of the TMR sensor preparation process is still needed to reduce the cost and improve the current detection sensitivity.

C. ME SENSING

The Hall and magnetoresistive sensors mentioned in the previous section have been widely used in magnetic field and current detection, but Hall sensors require a constant-current-source power supply with high stability and a weak Hall voltage of tens of μV/Oe, thus requiring a high-performance signal conditioning circuit. In contrast, ME sensors based on ME composites effectively avoid the above problems. Furthermore, they can simultaneously achieve wide-range, wideband ac and dc measurements with passive and self-energy extraction characteristics, which stand out in magnetic field detection and current detection tasks.

Scholars usually use the elastodynamic model, effective medium theory, and equivalent circuit model to describe ME phenomena. However, the first two models cannot describe the ME coupling effects under dynamic magnetic field excitation and are available only under static magnetic field excitation. Therefore, an approach based on the equivalent circuit model was proposed, and multiple vibration modes were defined, including the L-L, T-L, L-T, T-T, and push–pull modes. The principle of an ME material represented by the L-T mode with a sandwich structure is shown in Fig. 16(a) [143]. The piezoelectric material polarized along the thickness direction is sandwiched between two layers of magnetostrictive material polarized along the length direction and fixed by epoxy resin adhesive. The operation of this L-T-mode ME sensor can be divided into the following three steps. The magnetostrictive layer stretches along the length direction, and the piezoelectric layer vibrates in the same direction as the transfer of strain, thus generating a voltage in the thickness direction. Fig. 16(b) and (c) shows the equivalent circuit models of the two more commonly used vibration modes, L-T and L-L, respectively. Here, H is the applied magnetic field strength, φ_{m} is the magnetoelastic coupling coefficient, Z is the mechanical impedance of the composite, V is the voltage of the piezoelectric layer, φ_{p} is the electroelastic coupling coefficient, and C_0 is the static capacitance. This equivalent circuit model builds an analogy between mechanical and electrical parameters, making the physical phenomena in ME coupling materials easier to understand [144].

Dong et al. [145] proposed a current sensor with a toroidal structure of ME material to measure ac currents, and they used Terfenol-D rings magnetized along the circumferential direction and PZT rings in the corresponding polarization direction in their experiments. Subsequently, these scholars further improved the design of ME sensors, including by reducing the geometry and improving the measurement sensitivity. The improved sensor could achieve small current measurements at the nanoampere–microampere level at 100 kHz and exhibited high stability but could not achieve larger current measurements at the ampere level [146]. To solve the above

problem, Leung et al. [147] changed the circumferentially polarized PZT ring proposed by Dong et al. [146] to a thicker polarization ring with a slight increase in size so that it could achieve ampere-level current measurements at 30 kHz. To study the detection of larger ac currents, Zhang et al. [148] designed an ME sensor with an internal closed magnetic circuit, which consists of a high-permeability FeCuNbSiB nanocrystalline alloy ring and an L-T mode long-sheet Terfenol-D/PZT laminate composite; this sensor demonstrated large current measurements of 150 A in the range of 20 kHz. For dc measurements, Lou et al. [149] first proposed an ME sensor based on the T-T mode circular sheet-type Terfenol-D/PZT, which can measure dc currents up to 500 A with good linearity and without compensation.

From the developments of the above research, ME sensors have great potential for application in fields, such as transparent power grids and smart substations, including a wide variety of sensors and energy harvesting and transmission devices, due to their passive nature, small size, and high sensitivity. However, the theoretical development of ME sensors has been relatively slow, and there have been few theoretical studies and necessary device development reports on the coupling mechanism between magnetic, force, and electric multiphysical fields of composite materials, especially in the field of dc measurements. Therefore, future research on ME sensors should focus on accurate theoretical model construction and dc or magnetic field measurement scenarios.

D. SAW SENSING

The aforementioned measurement methods based on Hall sensing, magnetoresistive sensing, and ME sensing have matched well with the miniaturization and automation development of modern power systems and offer high reliability and stability advantages. However, these MEMS sensors based on magnetic field measurements often experience various unavoidable problems that make it difficult for them to adapt simultaneously to the needs of transparent power grids for responsiveness, sensitivity, reliability, insulation, environmental robustness, and wide range and wide frequency bands [150]. Therefore, SAW sensors with fast response capabilities can simultaneously meet the requirements of cost, sensitivity, and reliability, and are widely used in substations, CNC machines, and grid monitoring systems [151]. Furthermore, SAW sensors excite ultrasonic waves through the piezoelectric effect. Therefore, they are very sensitive to magnetic field perturbations on the surface and have great potential for application in passive wireless, high-temperature, high-voltage, and long-term monitoring environments [152].

The principles of SAW sensors can be divided into two main types. The first is a loaded structure combined with a magnetoresistive effect, as shown in Fig. 17(a). The sensor of this structure has a magnetoresistive load externally connected to the reflector to achieve passive wireless high-current measurement through the phase change in the reflected signal. Steindi et al. [153] proposed a loaded magnetic field

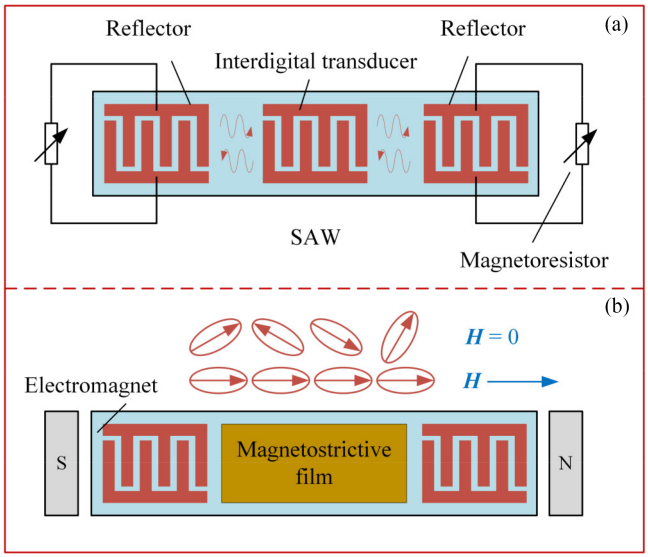

FIGURE 17. Schematic diagram of the structure of a SAW current sensor. (a) Magnetoresistive effect. (b) Magnetostrictive effect.

measurement device combining a giant magnetic impedance and a SAW sensor, which can operate stably in the temperature range of −60 °C to 200 °C where other types of sensors cannot adapt. Li et al. [154] proposed a loaded integrated acoustic surface wave sensor with simultaneous magnetic field, temperature, and humidity measurement capabilities; this sensor was fabricated using magnetic, thermal, and moisture-sensitive materials and demonstrated a sensitivity of 0.18 dB/Oe in magnetic field measurements and a maximum measurable current amplitude of 5 A. The relatively low sensitivity of such sensors is due to the fact that magnetoresistive materials based on the magnetoresistive effect tend to have lower magnetic sensitivity and resolution due to larger hysteresis.

To solve the above problems, the SAW current sensing method based on a highly magnetically sensitive and low-cost magnetostrictive film has been proposed by scholars, and its structure is shown in Fig. 17(b). In this current sensor, the magnetic field generated by the measured current causes strain in the magnetostrictive film, which affects the propagation speed of the surface wave and thus enables fast and accurate measurements of the current. The earliest acoustic surface wave sensors were mainly applied in magnetic field measurements, and Ganguly et al. [155] proposed a magnetostrictive acoustic surface wave device using an applied magnetic field to control the phase velocity by thermally evaporating 850 nm thick Ni onto a $LiNbO_3$ delay line; these researchers achieved good test results for a very high-frequency magnetic field of 70 MHz. For the measurement of small magnetic fields at the nT level, Hui et al. [156] proposed a MEMS resonant magnetic field sensor with an AIN/FeGaB bilayer structure with a quality factor of up to 511 and an electromechanical coupling coefficient of approximately 1.6%. A few years later, these scholars added Al_2O_3 as an intermediate layer of FeGaB

to reduce eddy current losses and achieved a sensitivity of 2.8 Hz/nT via 12 Oe dc magnetic fields [157]. Moreover, for the detection of large magnetic fields, Polewczyk et al. [158] proposed a multilayer magnetostrictive sensor structure with a $LiNbO_3$ substrate to obtain 0.5 T magnetic field measurements. Other recent studies have additionally increased the number of layers of magnetostrictive films but have used miniature magnetostrictive structures to achieve smaller and more sensitive magnetic field sensing [159], [160]. Few magnetostrictive sensors are used for current detection. Jia and Wang [161] proposed a high-sensitivity acoustic surface wave current sensor using a double delay line oscillator on a 128°YX-$LiNbO_3$ piezoelectric substrate as a sensing element. These investigators covered the surface of the piezoelectric substrate with a thin layer of SiO_2 to improve the temperature robustness. Wang et al. [162] analyzed the SAW current sensing mechanism based on the theory of acoustic propagation in layered media and the magnetostriction effect and developed a gated arrayed SAW current sensor using an iron–cobalt film. The sensor has a high sensitivity of 16.6 kHz/A and a low hysteresis error of 1.14%. Karapetyan et al. [163] proposed a sound surface wave current sensor with an FeNi thin film as the sensitive element; this sensor demonstrated high measurement sensitivity and could effectively measure impulse currents up to 1 GHz.

Due to the advantages of a wide range, high sensitivity, high reliability, adaptability to harsh environments, and wide application range, the SAW current sensor has broad application prospects in the future development of transparent power grids. However, although good experimental results have been achieved with magnetostrictive SAW sensors, the linearity and hysteresis errors of the current sensors are affected by the strong remanence and hysteresis of the magnetostrictive films, which hinder their practical application. Furthermore, most of the existing studies have focused on the preparation of sensor materials and anti-interference methods. Few studies have been proposed to optimize the sensor performance from an acoustic point of view, and the ultrasonic propagation characteristics represented by the SAW greatly affect the accuracy of the current measurements. Therefore, future research should further analyze the coupling characteristics of current and acoustic waves from an acoustic viewpoint based on the study of the relevant properties of magnetostrictive films.

E. SUMMARY

The transparent power grid focuses on integrating ICT with grid applications to fully understand the power grid status. Therefore, micro- and wireless sensors, including highly reliable and sensitive miniaturized MEMS current monitoring devices with easy information interaction, can be used as part of the critical sensing network for smart operation and maintenance of a transparent power grid.

Hall sensors have been widely used in the fields of grid current, magnetic field monitoring, substation operation and maintenance, and uninterruptible power system power supply monitoring due to their simple operation, high accuracy, and good linearity. However, Hall sensors have higher requirements for power supply stability and insulation, are more sensitive to the external environment and demonstrate greater power consumption. In contrast, magnetoresistive sensors have higher detection sensitivity, higher temperature stability, a wider linear range, and lower power consumption. However, magnetoresistive sensors still have greater difficulties in terms of low-frequency noise processing and high-current detection, and the reliance of the chip on a power supply makes it challenging to meet the demand for passive wireless current sensing in transparent power grids. Alternatively, ME sensors can be used to effectively solve passive wireless problems because of their small size and wide range. However, there is less research on ME sensors and no mature measurement theory or commercial products for reference. SAW current sensors have the advantages of a wide range, high sensitivity, high reliability, adaptability to harsh environments, and wide applicability, and can be used for integrated sensing of multiple physical quantities on the same chip. However, they rely on an external power supply to excite surface waves. In addition, to date, there have been few studies related to SAW current measurements, and no studies have been proposed to optimize the sensor performance from an acoustic point of view, thus limiting the development of this field.

Therefore, combined with the review of current sensing methods based on magnetic field measurements, in future research studies, the mutual compensation of multiple sensing methods needs to be explored in depth. Possible development directions include magnetoresistive and ME fusion of split-domain current measurement methods and the development of ultrasonic guided wave current sensors with better acoustic performance. Moreover, advanced deep learning technology can be used to rapidly process and aggregate measurement data to achieve online real-time intelligent sensing of the power grid's health status and improve its reliability.

VI. CHALLENGES AND DEVELOPMENTS

Current sensors play a vital role in power grid condition monitoring and are constantly being improved and upgraded as traditional power grids evolve into smart grids. Traditional shunts and Rogowski coils have been widely used in current measurements, and related technology has been developed to meet the wide-range, wide-band, and high-reliability current monitoring needs of traditional power grids. The infrastructure of the next-generation power grid is close to that of a smart grid. It is gradually transforming into a more advanced intelligent, market-oriented, and IoT-based transparent power grid, which also imposes higher requirements regarding the acquisition of power grid status information. New fiber optic sensing technology and magnetic field MEMS chip technology can significantly reduce the size and power consumption of sensors. The easy integration of multiple channels can significantly improve the sensor information collection efficiency and space utilization, allowing sensor manufacturing and maintenance costs to be effectively reduced, making it

easier to achieve cooperative control of multiple sensors and self-grouping collaborative current acquisition.

In addition to their original functions, intelligent devices in transparent power grids have the ability to perceive complex environmental information, process information, judge processing results, implement renewable information, and optimize operations. Based on this, the main intelligent application scenarios and performance requirements of high-current sensors in transparent power grids include the following.

1) *Intelligent electrical equipment:* In the intelligent electrical equipment scenario of end-edge-cloud collaboration, electrical devices, such as intelligent switchgears, pole-mounted switches, and circuit breakers, have higher requirements for accurate measurement of high currents. The measurement error range is generally 0.5% to 1%, and for high-current measurements in the kA range, an ability to detect current changes at the mA level is typically needed. In addition, the current measurement bandwidths of intelligent switchgears, pole-mounted switches, and circuit breakers depend on the application requirements. It is usually necessary to accurately measure currents in a specific frequency range, including from the power frequency to the kHz level.
2) *Intelligent transformers:* These are transformers that can interact with other devices or systems through a network in an intelligent system environment. Generally, traditional current transformers, shunts, and Rogowski coils can achieve flexible and reliable current measurement. However, intelligent transformers require real-time measurements of currents passing through them with millisecond-level response times, and the power consumption of the current sensors should reach the μW level to ensure continuous online operation.
3) *Transparent transmission lines:* Obtaining the amplitude, frequency, and waveform distortion index of transmission lines at different positions and times is an important way to achieve transparency of the transmission line status. Small and micro intelligent current sensors based on MEMS magnetic resistance can overcome the difficulties, high costs, poor real-time data acquisition, and low collection frequency associated with installing current transformers on high-voltage transmission lines. These devices can meet the requirements of μW power consumption, mm-level size, and 1% measurement accuracy.
4) *Mirror/digital twin power grid:* This refers to a mirrored physical power grid system in the digital space, which is continuously updated with changes in the physical power grid, enabling comprehensive perception and accurate prediction of the physical power grid. This application scenario relies on intelligent and wireless communication technologies with multiple network nodes and dynamic topology adaptation, as well as intelligent rapid processing methods, such as artificial intelligence, Big Data, ultra-real-time computing, parallel computing, and distributed computing.

However, the development of current sensing technology still faces several critical challenges in achieving fully intelligent and transparent sensing of the power grid state. These challenges include miniaturization and integration technologies for multisensor array measurements, low-power and self-energy extraction methods for microwatt passive sensors, wide-range and wide-band measurement methods for weak and large impulse current monitoring, highly reliable and sensitive sensor design concepts for complex electromagnetic and spatial environments, and intelligent and wireless communication technologies for multiple network nodes and dynamic topology adaptation. The development of these technologies and methods is essential for traditional power grids to upgrade to smart grids and is beneficial for developing transparent power grids with Internet technology at the core. Therefore, to meet the challenges facing the development of current sensing technology, improvements in the sensors themselves, the development of communication and networking technologies between sensors, and the study of intelligent and fast processing methods after communication is needed to improve the performance of current sensors.

In upgrading the sensor itself, exploring new methods of coupling physical quantities in addition to traditional physical effects, such as electro-optical effects and vibration, to achieve accurate measurement of current is a promising trend for the future. These methods include SAW current sensing via the magnetoacoustic coupling mechanism and ME laminated material current sensing methods using the ME mutual coupling mechanism. In addition, more advanced sensing material preparation methods with stronger environmental adaptation characteristics and new microsensor topology research are important directions for developing sensors. Furthermore, in communication and networking between sensors, the development of wireless sensing nodes with self-organization capability in wireless transmission technology and the proposed networked communication technology that adapts to rapid changes in network topology yield important improvement guidelines for the distribution of miniature current sensors. Moreover, the deep fusion of multisource heterogeneous information collected by many different types of current sensors to obtain the best estimate of the grid state is likewise an important guide for the future development of relay protection, grid control, and dispatching systems. In the development of current sensing decision terminals, digital twin technology can be used to combine real-time monitoring data with historical resources and build dynamic virtual interactive digital models through real-time state sensing and virtual reality, thus achieving virtual-real synchronization of digital models and current-monitoring distributed systems. In addition, the data-driven artificial intelligence-based approach can learn the common characteristics of the collected current data in detail, thus intelligently eliminating the interference of bad data and significantly improving the reliability of current measurement by sensors.

TABLE 5 Performance Comparison of Other Current Sensors

Method	Amplitude (kA)	Frequency (kHz)	Cost	Disadvantages	Advantages
Magnetic fluid optical sensing [164]	0.5	0.2	High	High light source power impact, limited performance available, large temperature drift	Good insulation performance, electrical isolation, small size, lightweight
Zero flux current transformer [137]	50	500	High	Difficult to apply to DC systems above 100 kV	High performance, high reliability
Electronic compensated transformer [165]	10	50	High	Relatively low reliability	Very high accuracy
DBI current transformer [166]	1	100	Medium	Higher cost, more complex structure, poor reliability	Can be used to convert the DC component of the frequency current
DC comparator [167]	300	DC	High	Difficult to detect zero flux accurately; magnetic error exists	Very high calibration accuracy to ppm level
Self-oscillating fluxgate [168]	0.7	DC~10^6	High	Costly, vulnerable to external strong magnetic fields, sensitivity affected by temperature	Simple modulation and demodulation circuit, high-cost performance, high sensitivity
Giant magnetic impedance [169]	0.002	1000	Low	Low zero-field sensitivity, position sensitive	High sensitivity and fast response time
Superconductivity [170]	10^{-11}—10^{-8}	10^6	High	Large volume, high demand for low temperature, unable to measure large currents	High sensitivity, high accuracy of very weak magnetic field measurement

VII. CONCLUSION

This article reviews the sensing technologies used in the current parametric state sensing of power grids, including the most widely used shunt, Rogowski coils with the widest range, fiber optic sensing with better anti-interference performance, and magnetic field MEMS sensing methods with a smaller size and lower energy consumption, based on the development logic of high-current detection technology for traditional smart transparent power grids. This article does not expand on other less commonly applied current measurement methods, such as dc comparators, self-oscillating flux gates, giant magnetic impedance, and superconducting current sensors. A comparison of the performances of these sensors is shown in Table 5 not provided in the main body of the article [164], [165], [166], [167], [168], [169], [170].

Current sensing technology based on shunts has the advantage of a simple measurement principle; it is highly accurate and largely unaffected by external magnetic fields. In addition, several commercial products have been widely used in industrial fields, and these products can achieve precision measurements for large dc currents at the 10-kA level and impulse currents at the 100-kA level. However, the shunt needs to connect a calibrated high-precision resistor to the main circuit of the measured circuit; therefore, this approach will affect the electrical parameters of the main circuit and create safety hazards. In addition, shunts generally exhibit characteristics, such as a large size, high power consumption in high-current measurements, temperature drift, residual inductance, and a skin effect, which have also limited their development.

Due to its wide measurement range, wide frequency band, high linearity, high stability, large saturation margin, small size, and safety brought by the open circuit on the secondary side, the Rogowski coil is more advantageous and is widely used in the measurement of steady-state ac, fault transient currents and large impulse currents up to the 1000-kA level. However, this sensor still has three problems: difficulty detecting dc or low-frequency currents, difficulty in performing accurate modeling, and difficulty in resisting interference with Rogowski coils at high frequencies. Furthermore, the size of Rogowski coils is generally large, and they are difficult to apply to small sensing scenarios. Fiber optic current transformers have recently gained wide application in dc transmission, including initial transitional optical current sensors based on a mixture of Rogowski coils and fiber optics, subsequent Faraday magneto-optical pure optical current sensors with smaller sizes and better temperature stability, and strain gauge optical current sensors. These fiber optic technology-based sensors also show unique advantages for large current measurements up to 500 kA. However, these sensors still exhibit issues, including lower reliability, linear birefringence, temperature drift, and vibration sensitivity. Therefore, conducting research on new optical materials and processes, proposing optical path design solutions with fewer devices, conducting proactive condition monitoring and early warning technology research, and adopting strict device screening and redundancy configuration measures will hopefully improve the environmental reliability of fiber optic current transformers.

Research on MEMS high-current sensing technology in transparent power grid state sensing has emerged based on the advantages of the noncontact nature, high isolation, and good environmental adaptability of magnetic field measurements. This technology can more easily be adapted to transparent power grids for the integration of multiparameter intelligent

sensing with control systems. Hall and magnetoresistive sensors can measure large currents above 10 kA as well as weak currents as low as 20 μA. However, this method still has major difficulties with respect to low-frequency noise processing and high-current detection, and the reliance of the chip on a power supply means that it is difficult to meet the demand for passive wireless current sensing in transparent power grids. To date, few studies have been conducted on ME sensors with passive radio characteristics and integratable SAW current sensors. Using these sensors, a maximum current of approximately 1 kA can be measured. Notably, ME sensors still perform well in the measurement of very weak currents as low as 10 nA and have lower power consumption, higher accuracy, and self-energy extraction. These sensors have great potential for wide-range current sensing in transparent power grids. However, few studies have proposed optimizing sensor performance from an acoustic perspective, thus limiting the development of this field.

REFERENCES

[1] K. Chen, Z. He, S. X. Wang, J. Hu, L. Li, and J. He, "Learning-based data analytics: Moving towards transparent power grids," *CSEE J. Power Energy Syst.*, vol. 4, no. 1, pp. 67–82, Mar. 2018, doi: 10.17775/CSEEJPES.2017.01070.

[2] L. Li et al., "Theoretical framework and key technologies of transparent power grid," *Strategic Study Chin. Acad. Eng.*, vol. 24, no. 4, pp. 32–43, 2022, doi: 10.15302/J-SSCAE-2022.04.025.

[3] G. Lou, "Theoretical modeling of magnetoelectric laminate composites and its application in current sensing," Ph.D. dissertation, Tsinghua Univ., Beijing, China, Jun. 2019.

[4] M. Kraft, "Measurement techniques of low-value high-current single-range current shunts from 15 Amps to 3000 Amps," *NCSLI Measure*, vol. 2, no. 1, pp. 44–49, Mar. 2007, doi: 10.1080/19315775.2007.11721357.

[5] H. Kato, M. Saito, K. Yoshino, A. Domae, S. Kiryu, and N.-H. Kaneko, "Shunt module development for simple DC high-current measurements," in *Proc. Conf. Precis. Electromagn. Meas.*, 2018, pp. 1–2.

[6] R. Malaric, *Instrumentation and Measurement in Electrical Engineering*. Boca Raton, FL, USA: BrownWalker Press, 2011.

[7] J. L. Everhart, *Engineering Properties of Nickel and Nickel Alloys*. New York, NY, USA: Plenum, 1971.

[8] S. Kon and T. Yamada, "Uncertainty evaluations of an AC shunt calibration system with a load effect reduction circuit," *IEEE Trans. Instrum. Meas.*, vol. 60, no. 7, pp. 2286–2291, Jul. 2011, doi: 10.1109/tim.2010.2103414.

[9] T. Bergsten and K.-E. Rydler, "Realization of absolute phase and AC resistance of current shunts by ratio measurements," *IEEE Trans. Instrum. Meas.*, vol. 68, no. 6, pp. 2041–2046, Jun. 2019, doi: 10.1109/TIM.2018.2882927.

[10] W. F. Praeg, "Stress sensitivity of Manganin resistor in high-current precision coaxial shunt," *IEEE Trans. Instrum. Meas.*, vol. 15, no. 4, pp. 234–242, Dec. 1966, doi: 10.1109/tim.1966.4313545.

[11] K. Lind, T. SØrsdal, and H. Slinde, "Design, modeling, and verification of high-performance AC–DC current shunts from inexpensive components," *IEEE Trans. Instrum. Meas.*, vol. 57, no. 1, pp. 176–181, Jan. 2008, doi: 10.1109/tim.2007.908602.

[12] B. Voljc, M. Lindic, B. Pinter, M. Kokalj, Z. Svetik, and R. Lapuh, "New design of coaxial current shunts for 50 A and 100 A," in *Proc. Conf. Precis. Electromagn. Meas.*, 2012, pp. 222–223.

[13] T. Yamada et al., "ECT evaluation by an error measurement system according to IEC 60044-8 and 61850-9-2," *IEEE Trans. Power Del.*, vol. 27, no. 3, pp. 1377–1384, Jul. 2012, doi: 10.1109/tpwrd.2012.2189590.

[14] T. Yamada, S. Kon, and T. Tadatsu, "Transresistance calibrations and temperature dependence evaluation of a magnetic bridge current sensor with shunt standards," *Meas. Sci. Technol.*, vol. 22, no. 10, Aug. 2011, Art. no. 105204, doi: 10.1088/0957-0233/22/10/105204.

[15] A. Dianov, "Recommendations and typical errors in design of power converter PCBs with shunt sensors," *IEEE Open J. Ind. Electron. Soc.*, vol. 3, pp. 329–338, 2022.

[16] S. Cui, S. Qiang, and Z. Ma, "Research on development status of pulse current shunts," *J. Astronautic Metrol. Meas.*, vol. 36, no. 6, pp. 82–88, Jul. 2016.

[17] J. Ge, L. Y. Tong, J. C. Geng, and H. Guang, "Research on thyristor conduction angle characteristics in transient process of TCSC," *Power Syst. Technol.*, vol. 25, no. 7, pp. 18–22, 2001.

[18] J. Liu, H. Zhong, and J. He, "Coaxial shunt for measuring ns level pulse high current," *High Voltage Appl.*, vol. 3, pp. 54–56, Aug. 1997.

[19] P. S. Filipski, M. Boecker, and M. Garcocz, "20-A to 100-A AC-DC coaxial current shunts for 100 kHz frequency range," *IEEE Trans. Instrum. Meas.*, vol. 57, no. 8, pp. 1637–1641, Aug. 2008, doi: 10.1109/TIM.2008.923783.

[20] K. Y. Sakharov, V. A. Turkin, O. V. Mikheev, M. Y. Denisov, V. L. Ugolev, and A. V. Sukhov, "A shunt for measurements of pulse currents based on a corrugated tube," *Meas. Techn.*, vol. 57, no. 12, pp. 1451–1456, Mar. 2015, doi: 10.1007/s11018-015-0648-8.

[21] R. Malewski, C. Nguyen, K. Feser, and N. Hylten-Cavallius, "Elimination of the skin effect error in heavy-current shunts," *IEEE Trans. Power App. Syst.*, vol. PAS-100, no. 3, pp. 1333–1340, Mar. 1981, doi: 10.1109/tpas.1981.316606.

[22] M. Sanoh, A. Mikata, K. Tokuno, M. Hanazawa, and H. Kakitani, "A calibration method for a commercial coaxial shunt at high pulse current," in *Proc. 29th Conf. Precis. Electromagn. Meas.*, 2014, pp. 630–631.

[23] R. Ferrero, M. Marracci, and B. Tellini, "Analytical study of high pulse current shunts," in *Proc. IEEE Int. Instrum. Meas. Technol. Conf.*, 2011, pp. 1–6.

[24] K. Schon, *High Impulse Voltage and Current Measurement Technique*. Berlin, Germany: Springer, 2013.

[25] F. Castelli, "The flat strap sandwich shunt," *IEEE Trans. Instrum. Meas.*, vol. 48, no. 5, pp. 894–898, Oct. 1999, doi: 10.1109/19.799642.

[26] J. Liu, Q. Xu, S. Li, Y. Yin, J. Feng, and X. Zhou, "Fold band shunt used in measuring the ns-grade pulse current," *High Voltage Eng.*, vol. 32, no. 5, pp. 57–59, Sep. 2006.

[27] C. Yu and D. Yu, "Study of step response performance of a disc shunt," *J. Xi'an Jiaotong Univ.*, vol. 25, no. 6, pp. 65–72, Sep. 1991.

[28] U. Pogliano, G. C. Bosco, and D. Serazio, "Coaxial shunts as AC–DC transfer standards of current," *IEEE Trans. Instrum. Meas.*, vol. 58, no. 4, pp. 872–877, Apr. 2009, doi: 10.1109/tim.2008.2008469.

[29] J. Zhang, Y. Jia, Y. Hu, W. Yue, and S. Zhang, "Design and application of measurement system of large current," *Metrol. Meas. Technol.*, vol. 35, no. 2, pp. 30–33, Nov. 2015.

[30] Y. Wu, C. Tian, Z. Zhang, B. Chen, S. Liu, and Y. Chen, "A novel current transformer based on virtual air gap and its basic measuring characteristics," *IEEE Trans. Power Del.*, vol. 38, no. 1, pp. 13–25, Feb. 2023, doi: 10.1109/TPWRD.2022.3179321.

[31] W. Li, "Study of sensor theory centered on Rogowski coil for heavy current measurement application," M.S. thesis, Huazhong Univ. Sci. Technol., Wuhan, China, 2005.

[32] W. Rogowski and W. Steinhaus, "Die Messung der magnetischen Spannung," *Arch. Elektrotechnik*, vol. 1, no. 4, pp. 141–150, Apr. 1912, doi: 10.1007/bf01656479.

[33] P. Niewczas, A. Cruden, W. C. Michie, W. I. Madden, and J. R. McDonald, "Error analysis of an optical current transducer operating with a digital signal processing system," *IEEE Trans. Instrum. Meas.*, vol. 49, no. 6, pp. 1254–1259, Dec. 2000, doi: 10.1109/19.893265.

[34] B. V. Djokic, "Improvements in the performance of a calibration system for Rogowski coils at high pulsed currents," *IEEE Trans. Instrum. Meas.*, vol. 66, no. 6, pp. 1636–1641, Jun. 2017, doi: 10.1109/tim.2016.2624578.

[35] A. N. Nanyan, M. Isa, H. A. Hamid, M. N. K. Hafizi Rohani, and B. Ismail, "The Rogowski coil sensor in high current application: A review," *IOP Conf. Ser. Mater. Sci. Eng.*, vol. 318, Mar. 2018, Art. no. 012054, doi: 10.1088/1757-899x/318/1/012054.

[36] M. E. Ibrahim and A. M. Abd-Elhady, "Power frequency AC voltage measurement based on double wound Rogowski coil," *High Voltage*, vol. 2, no. 2, pp. 129–135, Jun. 2017, doi: 10.1049/hve.2016.0091.

[37] S. Cao, J. Zhang, W. Zha, C. Zhao, B. Yang, and M. Zhu, "Experimental study on current measurement of Rogowski coil in a cryogenic environment," in *Proc. IEEE 3rd Int. Elect. Energy Conf.*, 2019, pp. 1264–1269, doi: 10.1109/CIEEC47146.2019.CIEEC-2019463.

[38] J. A. J. Pettinga and J. Siersema, "A polyphase 500 kA current measuring system with Rogowski coils," *IEE Proc. B (Electric Power Appl.)*, vol. 130, no. 5, pp. 360–363, Sep. 1983, doi: 10.1049/ip-b.1983.0054.

[39] W. Limcharoen and P. Yutthagowith, "Rogowski coil with an active integrator for measurement of switching impulse current," in *Proc. 10th Int. Conf. Elect. Eng./Electron., Comput., Telecommun. Inf. Technol.*, 2013, pp. 1–4, doi: 10.1109/ECTICon.2013.6559578.

[40] M. H. Samimi, A. Mahari, M. A. Farahnakian, and H. Mohseni, "The Rogowski coil principles and applications: A review," *IEEE Sensors J.*, vol. 15, no. 2, pp. 651–658, Feb. 2015, doi: 10.1109/jsen.2014.2362940.

[41] Y. Shi, Z. Xin, P. C. Loh, and F. Blaabjerg, "A review of traditional helical to recent miniaturized printed circuit board Rogowski coils for power-electronic applications," *IEEE Trans. Power Electron.*, vol. 35, no. 11, pp. 12207–12222, Nov. 2020, doi: 10.1109/tpel.2020.2984055.

[42] L. Ferkovic, D. Ilic, and I. Lenicek, "Influence of axial inclination of the primary conductor on mutual inductance of a precise Rogowski coil," *IEEE Trans. Instrum. Meas.*, vol. 64, no. 11, pp. 3045–3054, Nov. 2015, doi: 10.1109/tim.2015.2444254.

[43] R. Wang, S. Prabhakaran, W. Burdick, and R. Nicholas, "Rogowski current sensor design and analysis based on printed circuit boards (PCB)," in *Proc. IEEE Energy Convers. Congr. Expo.*, 2014, pp. 3206–3211.

[44] M. Habrych, G. Wisniewski, B. Miedzinski, A. Lisowiec, and Z. Fjalkowski, "HDI PCB Rogowski coils for automated electrical power system applications," *IEEE Trans. Power Del.*, vol. 33, no. 4, pp. 1536–1544, Aug. 2018, doi: 10.1109/tpwrd.2017.2765400.

[45] Y. Lu, X. Zhang, H. Shen, W. Zhang, and L. Qi, "A segmented Rogowski coils based noninvasive monitoring method of current imbalance in press pack IGBTs," *IEEE Trans. Power Electron.*, vol. 38, no. 10, pp. 12320–12324, Oct. 2023, doi: 10.1109/TPEL.2023.3292263.

[46] M. Marracci, B. Tellini, C. Zappacosta, and G. Robles, "Critical parameters for mutual inductance between Rogowski coil and primary conductor," *IEEE Trans. Instrum. Meas.*, vol. 60, no. 2, pp. 625–632, Feb. 2011, doi: 10.1109/tim.2010.2051591.

[47] J. A. Ardila-Rey et al., "Behavior of an inductive loop sensor in the measurement of partial discharge pulses with variations in its separation from the primary conductor," *Sensors*, vol. 18, no. 7, Jul. 2018, Art. no. 2324, doi: 10.3390/s18072324.

[48] E. Farjah, H. Givi, and T. Ghanbari, "Application of an efficient Rogowski coil sensor for switch fault diagnosis and capacitor ESR monitoring in nonisolated single-switch DC–DC converters," *IEEE Trans. Power Electron.*, vol. 32, no. 2, pp. 1442–1456, Feb. 2017, doi: 10.1109/tpel.2016.2552039.

[49] G. M. Hashmi, M. Lehtonen, and A. Ametani, "Modeling and experimental verification of covered-conductor for PD detection in overhead distribution networks -modeling covered-conductor overhead distribution networks for PD detection," *IEEJ Trans. Power Energy*, vol. 130, no. 7, pp. 670–678, 2010, doi: 10.1541/ieejpes.130.670.

[50] T. Tao, Z. Zhao, W. Ma, Q. Pan, and A. Hu, "Design of PCB Rogowski coil and analysis of anti-interference property," *IEEE Trans. Electromagn. Compat.*, vol. 58, no. 2, pp. 344–355, Apr. 2016, doi: 10.1109/temc.2013.2252906.

[51] M. Shafiq, L. Kutt, M. Lehtonen, T. Nieminen, and M. Hashmi, "Parameters identification and modeling of high-frequency current transducer for partial discharge measurements," *IEEE Sensors J.*, vol. 13, no. 3, pp. 1081–1091, Mar. 2013, doi: 10.1109/jsen.2012.2227712.

[52] T. Guillod, D. Gerber, J. Biela, and A. Muesing, "Design of a PCB Rogowski coil based on the PEEC method," in *Proc. 7th Int. Conf. Integr. Power Electron. Syst.*, 2012, pp. 1–6.

[53] C. Hewson and J. Aberdeen, "An improved Rogowski coil configuration for a high speed, compact current sensor with high immunity to voltage transients," in *Proc. IEEE Appl. Power Electron. Conf. Expo.*, 2018, pp. 571–578.

[54] M. E. Ibrahim and A. M. Abd-elhady, "Differential reconstruction method for power frequency AC current measurement using Rogowski coil," *IEEE Sensors J.*, vol. 16, no. 23, pp. 8420–8425, Dec. 2016, doi: 10.1109/jsen.2016.2614352.

[55] E. Lesniewska and A. Lisowiec, "Estimation of influence of external magnetic field on new technology current-to-voltage transducers operating in protection system of AC power networks," *IEEE Trans. Power Del.*, vol. 31, no. 2, pp. 541–550, Apr. 2016, doi: 10.1109/tpwrd.2015.2454051.

[56] J. D. Ramboz, "Machinable Rogowski coil, design, and calibration," *IEEE Trans. Instrum. Meas.*, vol. 45, no. 2, pp. 511–515, Apr. 1996, doi: 10.1109/19.492777.

[57] R. V. Carvalho, D. de Andrade Ussuna, V. S. Filho, L. F. R. Barrozo, M. J. do Couto Bonfim, and R. Martins, "Electronic instrumentation applied to the indirect measurement of 230 kV overhead transmission lines ampacity," in *Proc. 11th Int. Conf. Power, Energy Elect. Eng.*, 2021, pp. 8–14, doi: 10.1109/CPEEE51686.2021.9383352.

[58] L. Kojovic, "PCB Rogowski coils benefit relay protection," *IEEE Comput. Appl. Power*, vol. 15, no. 3, pp. 50–53, Jul. 2002, doi: 10.1109/mcap.2002.1018823.

[59] Z. Yan and L. Hongbin, "The reliable design of PCB Rogowski coil current transformer," in *Proc. Int. Conf. Power Syst. Technol.*, 2006, pp. 1–4.

[60] J. N. Fritz, C. Neeb, and R. W. D. Doncker, "A PCB integrated differential Rogowski coil for non-intrusive current measurement featuring high bandwidth and dv/dt immunity," in *Proc. Power Energy Student Summit*, 2015, Art. no. S05.2.

[61] Y. Cheng, Y. Sha, S. Wei, J. Bi, W. Chang, and X. Ma, "Novel spiral-gap shielding shell for a Rogowski current sensor," *IEEE Trans. Electromagn. Compat.*, vol. 64, no. 4, pp. 1058–1066, Aug. 2022, doi: 10.1109/temc.2022.3157164.

[62] M. J. A. M. van Helvoort and D. W. Harberts, "Low-frequency electromagnetic shielding and scattering of multiple cylindrical shells," *IEEE Trans. Electromagn. Compat.*, vol. 63, no. 1, pp. 46–56, Feb. 2021, doi: 10.1109/temc.2020.3011757.

[63] M. Maddah-Ali, S. H. H. Sadeghi, and M. Dehmollaian, "Efficient method for calculating the shielding effectiveness of axisymmetric multilayered composite enclosures," *IEEE Trans. Electromagn. Compat.*, vol. 62, no. 1, pp. 218–228, Feb. 2020, doi: 10.1109/temc.2019.2894989.

[64] A. Shourvarzi and M. Joodaki, "Shielding effectiveness measurement for extremely small dimension enclosures," *IEEE Trans. Electromagn. Compat.*, vol. 61, no. 6, pp. 1740–1745, Dec. 2019, doi: 10.1109/temc.2018.2882893.

[65] J. Wang, "Switching-cycle control and sensing techniques for high-density SiC-based modular converters," M.S. thesis, Dept. Elect. Eng. Virginia Polytech., Indiana State Univ., Blacksburg, VA, USA, 2017.

[66] E.-P. Suomalainen and J. K. Hallstrom, "Onsite calibration of a current transformer using a Rogowski coil," *IEEE Trans. Instrum. Meas.*, vol. 58, no. 4, pp. 1054–1058, Apr. 2009, doi: 10.1109/tim.2008.2007031.

[67] Y. Zhang, J. Liu, G. Bai, and J. Feng, "Analysis of damping resistor's effects on pulse response of self-integrating Rogowski coil with magnetic core," *Measurement*, vol. 45, no. 5, pp. 1277–1285, Jun. 2012, doi: 10.1016/j.measurement.2012.01.009.

[68] T. Kawabata, S. Yanagawa, H. Takahashi, and K. Yamamoto, "Development of a shunt lightning current measuring system using a Rogowski coil," *Elect. Power Syst. Res.*, vol. 118, pp. 110–113, Jan. 2015, doi: 10.1016/j.epsr.2014.07.015.

[69] O. Poncelas, J. A. Rosero, J. Cusido, J. A. Ortega, and L. Romeral, "Motor fault detection using a Rogowski sensor without an integrator," *IEEE Trans. Ind. Electron.*, vol. 56, no. 10, pp. 4062–4070, Oct. 2009, doi: 10.1109/tie.2009.2025715.

[70] S. Wang, X. Cao, and L. Chen, "Study of ECT based on Rogowski coil used in smart substation," in *Proc. IEEE 7th Int. Power Eng. Optim. Conf.*, 2013, pp. 61–65.

[71] L. A. Kojovic, "Applications of Rogowski coils for advanced power system solutions," in *Proc. 18th Int. Conf. Exhib. Electricity Distrib.*, 2005, pp. 1–4.

[72] J. P. Dupraz, A. Fanget, W. Grieshaber, and G. F. Montillet, "Rogowski coil: Exceptional current measurement tool for almost any application," in *Proc. IEEE Power Eng. Soc. Gen. Meeting*, 2007, pp. 1–8.

[73] S. Sharifinia, M. Allahbakhshi, T. Ghanbari, A. Akbari, and H. R. Mirzaei, "A new application of Rogowski coil sensor for partial discharge localization in power transformers," *IEEE Sensors J.*, vol. 21, no. 9, pp. 10743–10751, May 2021, doi: 10.1109/jsen.2021.3062770.

[74] T. Funk, J. Groeger, and B. Wicht, "An integrated and galvanically isolated DC-to-15.3 MHz hybrid current sensor," in *Proc. IEEE Appl. Power Electron. Conf. Expo.*, 2019, pp. 1010–1013.

[75] R. Hao, "Optical fiber current sensor based on MEMS technology and magnetic field gradient force," Ph.D. dissertation, Harbin Univ. Sci. Technol., Harbin, China, 2021.

[76] S. Zhang, "Research on the principle of temperature compensation of GMM-FBG current sensor based on all-fiber MZI," M.S. thesis, Lanzhou Jiaotong Univ., Lanzhou, China, 2021.

[77] Q. Huang, C. Zhang, Q. Liu, Y. Ning, and Y. Cao, "New type of fiber optic sensor network for smart grid interface of transmission system," in *Proc. IEEE PES Gen. Meeting*, 2010, pp. 1–5, doi: 10.1109/PES.2010.5589596.

[78] N. A. Pilling, R. Holmes, and G. R. Jones, "Optically powered hybrid current measurement system," *Electron. Lett.*, vol. 29, no. 12, pp. 1049–1051, Jun. 1993, doi: 10.1049/el:19930700.

[79] J. D. Bull, N. A. F. Jaeger, and F. Rahmatian, "A new hybrid current sensor for high-voltage applications," *IEEE Trans. Power Del.*, vol. 20, no. 1, pp. 32–38, Jan. 2005, doi: 10.1109/tpwrd.2004.833889.

[80] J. Xie, X. Han, Z. Song, and J. Luo, "Development of an optical digitized local control and measurement system applied to pulsed high magnetic field facility," *IEEE Trans. Appl. Supercond.*, vol. 20, no. 3, pp. 1777–1780, Jun. 2010, doi: 10.1109/tasc.2010.2041442.

[81] P. Orr et al., "An optically-interrogated Rogowski coil for passive, multiplexable current measurement," *IEEE Sensors J.*, vol. 13, no. 6, pp. 2053–2054, Jun. 2013, doi: 10.1109/jsen.2013.2252614.

[82] P. Wei, C. Cheng, L. Deng, and H. Huang, "A hybrid electro-optic current transducer using a photodiode-based primary supply," *IEEE Sensors J.*, vol. 17, no. 9, pp. 2713–2717, May 2017, doi: 10.1109/jsen.2017.2674974.

[83] Y. N. Ning, Z. P. Wang, A. W. Palmer, K. T. V. Grattan, and D. A. Jackson, "Recent progress in optical current sensing techniques," *Rev. Sci. Instrum.*, vol. 66, no. 5, pp. 3097–3111, May 1995, doi: 10.1063/1.1145537.

[84] A. Papp and H. Harms, "Magnetooptical current transformer. 1: Principles," *Appl. Opt.*, vol. 19, no. 22, pp. 3729–3734, Nov. 1980, doi: 10.1364/AO.19.003729.

[85] J. Wu and X. Zhang, "Recent progress of all fiber optic current transformers," in *Proc. 7th Int. Forum Elect. Eng. Automat.*, 2020, pp. 134–143.

[86] J. N. Blake, *All-Fiber In-Line Sagnac Interferometer Current Sensor*. Bellingham, WA, USA: Int. Soc. Opt. Photon., 1995.

[87] J. Blake, P. Tantaswadi, and R. T. de Carvalho, "In-line Sagnac interferometer current sensor," *IEEE Trans. Power Del.*, vol. 11, no. 1, pp. 116–121, Jan. 1996, doi: 10.1109/61.484007.

[88] C. He et al., "Design and experimental study on temperature control circuit of semiconductor laser," *Electron. Meas. Technol.*, vol. 40, no. 8, pp. 27–31, Dec. 2017.

[89] H. Yang, L. Qiao, Y. Yang, W. Huang, and S. Sun, "Thermally induced error analysis and suppression of optic fiber delay loop in the different variable rate of temperature," *Optik*, vol. 193, Sep. 2019, Art. no. 162994, doi: 10.1016/j.ijleo.2019.162994.

[90] H. Hu, J. Huang, L. Xia, Z. Yan, and S. Peng, "The compensation of long-term temperature induced error in the all fiber current transformer through optimizing initial phase delay in λ/4 wave plate," *Microw. Opt. Technol. Lett.*, vol. 61, no. 7, pp. 1769–1773, Feb. 2019, doi: 10.1002/mop.31793.

[91] H. Yang, W. Huang, S. Jiao, X. Sun, W. Hong, and L. Qiao, "Temperature independent polarization-maintaining photonic crystal fiber with regular pentagon air hole distribution," *Optik*, vol. 185, pp. 390–396, May 2019, doi: 10.1016/j.ijleo.2019.03.120.

[92] H. Zhang et al., "A loop all-fiber current sensor based on single-polarization single-mode couplers," *Sensors*, vol. 17, no. 11, Nov. 2017, Art. no. 2674, doi: 10.3390/s17112674.

[93] K. Bohnert, C.-P. Hsu, L. Yang, A. Frank, G. M. Müller, and P. Gabus, "Polarimetric fiber-optic current sensor with integrated-optic polarization splitter," *J. Lightw. Technol.*, vol. 36, no. 11, pp. 2161–2165, Jul. 2018, doi: 10.1109/JLT.2018.2803807.

[94] A. J. Rogers, "Optical technique for measurement of current at high voltage," *Proc. Inst. Elect. Eng.*, vol. 120, no. 2, pp. 261–267, Feb. 1973, doi: 10.1049/piee.1973.0057.

[95] X. Ma and C. Luo, "A method to eliminate birefringence of a magneto-optic AC current transducer with glass ring sensor head," *IEEE Trans. Power Del.*, vol. 13, no. 4, pp. 1015–1019, Oct. 1998, doi: 10.1109/61.714435.

[96] T. Sato, G. Takahashi, and Y. Inui, "Method and apparatus for optically measuring a current," U.S. Patent 4564754, 1986.

[97] T. D. Maffetone and T. M. McClelland, "345 kV substation optical current measurement system for revenue metering and protective relaying," *IEEE Trans. Power Del.*, vol. 6, no. 4, pp. 1430–1437, Oct. 1991, doi: 10.1109/61.97673.

[98] P. Niewczas, W. C. Michie, I. W. Madden, A. Cruden, and J. R. McDonald, "Field evaluation of FR5 glass optical current transducer," in *Proc. SPIE Int. Soc. Opt. Eng.*, 2000, pp. 146–155.

[99] M. Wang, J. Zhao, S. Liu, F. Liu, X. Wan, and P. Zhang, "Optical current sensor immune to reflection phase shift based on graded-index magneto-optical glass," *Appl. Opt.*, vol. 48, no. 32, pp. 6264–6270, Nov. 2009, doi: 10.1364/AO.48.006264.

[100] N. E. Fisher, P. J. Henderson, and D. A. Jackson, "The interrogation of a conventional current transformer using an in-fibre Bragg grating," *Meas. Sci. Technol.*, vol. 8, no. 10, pp. 1080–1084, Jan. 1997, doi: 10.1088/0957-0233/8/10/007.

[101] X. Wang, X. Li, Z. Du, and J. Chen, "Design of interferometric fiber-optic weak DC electric-field sensor," *Chin. J. Sensors Actuators*, vol. 21, no. 5, pp. 765–768, Jul. 2008.

[102] L. M. B. Soares, J. D. Lopez Vargas, R. C. da Silva, B. Allil, A. Dante, and M. M. Werneck, "Optical magnetostrictive current sensor based on in-fiber Fabry–Pérot cavity," *IEEE Sensors J.*, vol. 22, no. 21, pp. 20499–20507, Nov. 2022, doi: 10.1109/JSEN.2022.3206949.

[103] D. Satpathi, J. A. Moore, and M. G. Ennis, "Design of a terfenol-D based fiber-optic current transducer," *IEEE Sensors J.*, vol. 5, no. 5, pp. 1057–1065, Oct. 2005, doi: 10.1109/jsen.2005.850996.

[104] D. Reilly, A. J. Willshire, G. Fusiek, P. Niewczas, and J. R. McDonald, "A Fiber-Bragg-grating-based sensor for simultaneous AC current and temperature measurement," *IEEE Sensors J.*, vol. 6, no. 6, pp. 1539–1542, Dec. 2006, doi: 10.1109/jsen.2006.883858.

[105] J. Han et al., "Temperature-compensated magnetostrictive current sensor based on the configuration of dual fiber Bragg gratings," *J. Lightw. Technol.*, vol. 35, no. 22, pp. 4910–4915, Nov. 2017, doi: 10.1109/jlt.2017.2766119.

[106] L. Jiang, "The research on temperature compensation system for GMM-FBG current transformer based on FPGA," Ph.D. dissertation, Harbin Univ. Sci. Technol., Harbin, China, 2013.

[107] K. S. Chiang, R. Kancheti, and V. Rastogi, "Temperature-compensated fiber-Bragg-grating-based magnetostrictive sensor for DC and AC currents," *Opt. Eng.*, vol. 42, no. 7, pp. 1906–1909, Jul. 2003, doi: 10.1117/1.1576533.

[108] J. Mora, L. Martínez-León, A. Díez, J. L. Cruz, and M. V. Andrés, "Simultaneous temperature and ac-current measurements for high voltage lines using fiber Bragg gratings," *Sensors Actuators A Phys.*, vol. 125, no. 2, pp. 313–316, Jan. 2006, doi: 10.1016/j.sna.2005.10.003.

[109] P. M. Cavaleiro, F. M. Araújo, and A. B. Lobo Ribeiro, "Metal-coated fibre Bragg grating sensor for electric current metering," *Electron. Lett.*, vol. 34, no. 11, pp. 1133–1135, May 1998, doi: 10.1049/el:19980785.

[110] S. Nodehi, W. S. Mohammed, H. Ahmad, and S. W. Harun, "Realization of spectral tunable filter based on thermal effect in microfiber structure," *Opt. Fiber Technol.*, vol. 28, pp. 38–41, Mar. 2016, doi: 10.1016/j.yofte.2016.01.001.

[111] M. Belal, Z. Q. Song, Y. Jung, G. Brambilla, and T. Newson, "An interferometric current sensor based on optical fiber micro wires," *Opt. Exp.*, vol. 18, no. 19, pp. 19951–19956, Sep. 2010, doi: 10.1364/OE.18.019951.

[112] S.-C. Yan, B.-C. Zheng, J.-H. Chen, F. Xu, and Y.-Q. Lu, "Optical electrical current sensor utilizing a graphene-microfiber-integrated coil resonator," *Appl. Phys. Lett.*, vol. 107, no. 5, Aug. 2015, Art. no. 053502, doi: 10.1063/1.4928247.

[113] A. Sulaiman, S. W. Harun, I. Aryangar, and H. Ahmad, "DC current sensing capability of microfibre Mach-Zehnder interferometer," *Electron. Lett.*, vol. 48, no. 15, pp. 943–945, Jul. 2012, doi: 10.1049/el.2012.1435.

[114] A. A. Jasim, S. W. Harun, M. Z. Muhammad, H. Arof, and H. Ahmad, "Current sensor based on inline microfiber Mach–Zehnder interferometer," *Sensors Actuators A Phys.*, vol. 192, pp. 9–12, Apr. 2013, doi: 10.1016/j.sna.2012.12.012.

[115] X. Song, K. Liu, and J. Shen, *Research and Design of New Generation Intelligent Substation*. Beijing, China: China Electric Power Press, 2014.

[116] T. Waeckerlé, H. Fraisse, Q. Furnemont, and F. Bloch, "Upgrade Fe-50%Ni alloys for open-loop DC current sensor: Design and alloy-potential characteristics," *J. Magnetism Magn. Mater.*, vol. 304, no. 2, pp. e850–e852, Sep. 2006, doi: 10.1016/j.jmmm.2006.03.015.

[117] R. S. Popovic, P. M. Drljaca, and P. Kejik, "CMOS magnetic sensors with integrated ferromagnetic parts," *Sensors Actuators A Phys.*, vol. 129, no. 1-2, pp. 94–99, May 2004, doi: 10.1016/j.sna.2005.11.048.

[118] V. Frick, P. Poure, L. Hébrard, F. Anstotz, and F. Braun, "Electromagnetically compatible CMOS auto-balanced current sensor for highly integrated power control System-on-chip," *Int. J. Electron.*, vol. 94, no. 1, pp. 9–22, Jan. 2007, doi: 10.1080/00207210600924712.

[119] G. D'Antona, L. Di Rienzo, R. Ottoboni, and A. Manara, "Processing magnetic sensor array data for AC current measurement in multiconductor systems," *IEEE Trans. Instrum. Meas.*, vol. 50, no. 5, pp. 1289–1295, Oct. 2001, doi: 10.1109/19.963199.

[120] L. Dalessandro, N. Karrer, and J. W. Kolar, "High-performance planar isolated current sensor for power electronics applications," *IEEE Trans. Power Electron.*, vol. 22, no. 5, pp. 1682–1692, Sep. 2007, doi: 10.1109/tpel.2007.904198.

[121] V. Mosser, N. Matringe, and Y. Haddab, "A spinning current circuit for hall measurements down to the nanotesla range," *IEEE Trans. Instrum. Meas.*, vol. 66, no. 4, pp. 637–650, Apr. 2017, doi: 10.1109/tim.2017.2649858.

[122] M. Crescentini, M. Marchesi, A. Romani, M. Tartagni, and P. A. Traverso, "A broadband, on-chip sensor based on hall effect for current measurements in smart power circuits," *IEEE Trans. Instrum. Meas.*, vol. 67, no. 6, pp. 1470–1485, Jun. 2018, doi: 10.1109/tim.2018.2795248.

[123] M. Blagojevic, U. Jovanovic, I. Jovanovic, D. Mancic, and R. Popovic, "Coreless open-loop current transducers based on hall effect sensor CSA-1V," *Facta Univ. Ser. Electron. Energetics*, vol. 29, no. 4, pp. 489–507, Jan. 2016, doi: 10.2298/fuee1604489b.

[124] F. Zapf, R. Weiss, A. Itzke, R. Gordon, and R. Weigel, "Mechanically flexible sensor array for current measurement," *IEEE Trans. Instrum. Meas.*, vol. 69, no. 10, pp. 8554–8561, Oct. 2020, doi: 10.1109/tim.2020.2993119.

[125] N. George and S. Gopalakrishna, "Design and development of a differential current probe with high misalignment tolerance," *IEEE Sensors J.*, vol. 19, no. 16, pp. 7035–7042, Aug. 2019, doi: 10.1109/jsen.2019.2912508.

[126] A. Patel and M. Ferdowsi, "Current sensing for automotive electronics—A survey," *IEEE Trans. Veh. Technol.*, vol. 58, no. 8, pp. 4108–4119, Oct. 2009, doi: 10.1109/tvt.2009.2022081.

[127] X. Liu et al., "Overview of spintronic sensors with Internet of Things for smart living," *IEEE Trans. Magn.*, vol. 55, no. 11, Nov. 2019, Art. no. 0800222, doi: 10.1109/tmag.2019.2927457.

[128] Z. Zhenhong, O. Syuji, A. Osamu, and K. Hideto, "Development of the highly precise magnetic current sensor module of +/−300 a utilizing AMR element with bias-magnet," *IEEE Trans. Magn.*, vol. 51, no. 1, Jan. 2015, Art. no. 4000205, doi: 10.1109/tmag.2014.2359209.

[129] P. Mlejnek and P. Ripka, "AMR yokeless current sensor with improved accuracy," *Procedia Eng.*, vol. 168, pp. 900–903, Dec. 2016, doi: 10.1016/j.proeng.2016.11.301.

[130] S. J. Nibir and B. Parkhideh, "Magnetoresistor with planar magnetic concentrator as wideband contactless current sensor for power electronics applications," *IEEE Trans. Ind. Electron.*, vol. 65, no. 3, pp. 2766–2774, Mar. 2018, doi: 10.1109/tie.2017.2739711.

[131] M. N. Baibich et al., "Giant magnetoresistance of (001)Fe/(001)Cr magnetic superlattices," *Phys. Rev. Lett.*, vol. 61, no. 21, pp. 2472–2475, Nov. 1988, doi: 10.1103/PhysRevLett.61.2472.

[132] M. Vieth, W. Clemens, H. van den Berg, G. Rupp, J. Wecker, and M. Kroeker, "Contactless current detection with GMR sensors based on an artificial antiferromagnet (AAF) subsystem," *Sensors Actuators A Phys.*, vol. 81, no. 1-3, pp. 44–48, Apr. 2000, doi: 10.1016/s0924-4247(99)00113-2.

[133] H. Beltran, C. Reig, V. Fuster, D. RamÍrez, and M. D. Cubells-BeltrÁn, "Modeling of magnetoresistive-based electrical current sensors: A technological approach," *IEEE Sensors J.*, vol. 7, no. 11, pp. 1532–1537, Nov. 2007, doi: 10.1109/jsen.2007.908241.

[134] N. George and S. Gopalakrishna, "Development of a new low-cost and reliable core-less current probe for conductor with reduced access," *IEEE Sensors J.*, vol. 17, no. 14, pp. 4619–4627, Jul. 2017, doi: 10.1109/jsen.2017.2710263.

[135] M. Julliere, "Tunneling between ferromagnetic films," *Phys. Lett. A*, vol. 54, no. 3, pp. 225–226, Sep. 1975, doi: 10.1016/0375-9601(75)90174-7.

[136] J. S. Moodera, L. R. Kinder, T. M. Wong, and R. Meservey, "Large magnetoresistance at room temperature in ferromagnetic thin film tunnel junctions," *Phys. Rev. Lett.*, vol. 74, no. 16, pp. 3273–3276, Apr. 1995, doi: 10.1103/PhysRevLett.74.3273.

[137] S. Ziegler, R. C. Woodward, H. H.-C. Iu, and L. J. Borle, "Current sensing techniques: A review," *IEEE Sensors J.*, vol. 9, no. 4, pp. 354–376, Apr. 2009, doi: 10.1109/jsen.2009.2013914.

[138] H. Zhang, F. Li, H. Guo, Z. Yang, and N. Yu, "Current measurement with 3-D coreless TMR sensor array for inclined conductor," *IEEE Sensors J.*, vol. 19, no. 16, pp. 6684–6690, Aug. 2019, doi: 10.1109/JSEN.2019.2914939.

[139] H. Yu, Z. Qian, H. Liu, and J. Qu, "Circular array of magnetic sensors for current measurement: Analysis for error caused by position of conductor," *Sensors*, vol. 18, no. 2, Feb. 2018, Art. no. 578, doi: 10.3390/s18020578.

[140] A. H. Khawaja, Q. Huang, and Y. Chen, "A novel method for wide range electric current measurement in gas-insulated switchgears with shielded magnetic measurements," *IEEE Trans. Instrum. Meas.*, vol. 68, no. 12, pp. 4712–4722, Dec. 2019, doi: 10.1109/tim.2019.2897039.

[141] H. Zhang, F. Li, H. Guo, Z. Yang, and N. Yu, "Current measurement with 3-D coreless TMR sensor array for inclined conductor," *IEEE Sensors J.*, vol. 19, no. 16, pp. 6684–6690, Aug. 2019, doi: 10.1109/jsen.2019.2914939.

[142] J. Li, H. Liu, and T. Bi, "Tunnel magnetoresistance-based noncontact current sensing and measurement method," *IEEE Trans. Instrum. Meas.*, vol. 71, 2022, Art. no. 9503609, doi: 10.1109/tim.2022.3152240.

[143] S. Dong, J.-F. Li, and D. Viehland, "Longitudinal and transverse magnetoelectric voltage coefficients of magnetostrictive/piezoelectric laminate composite: Experiments," *IEEE Trans. Ultrasonics, Ferroelect., Freq. Control*, vol. 51, no. 7, pp. 794–799, Jul. 2004, doi: 10.1109/tuffc.2004.1320738.

[144] S. Dong, J. F. Li, and D. Viehland, "Longitudinal and transverse magnetoelectric voltage coefficients of magnetostrictive/piezoelectric laminate composite: Theory," *IEEE Trans. Ultrasonics, Ferroelect., Freq. Control*, vol. 50, no. 10, pp. 1253–1261, Oct. 2003, doi: 10.1109/tuffc.2003.1244741.

[145] S. Dong, J.-F. Li, and D. Viehland, "Vortex magnetic field sensor based on ring-type magnetoelectric laminate," *Appl. Phys. Lett.*, vol. 85, no. 12, pp. 2307–2309, Sep. 2004, doi: 10.1063/1.1791732.

[146] S. Dong et al., "Circumferential-mode, quasi-ring-type, magnetoelectric laminate composite—A highly sensitive electric current and/or vortex magnetic field sensor," *Appl. Phys. Lett.*, vol. 86, no. 18, May 2005, Art. no. 182506, doi: 10.1063/1.1923184.

[147] C. M. Leung, S. W. Or, S. Zhang, and S. L. Ho, "Ring-type electric current sensor based on ring-shaped magnetoelectric laminate of epoxy-bonded Tb0.3Dy0.7Fe1.92 short-fiber/NdFeB magnet magnetostrictive composite and Pb(Zr, Ti)O3 piezoelectric ceramic," *J. Appl. Phys.*, vol. 107, no. 9, May 2010, Art. no. 09D918, doi: 10.1063/1.3360349.

[148] J. Zhang et al., "High-resolution current sensor utilizing nanocrystalline alloy and magnetoelectric laminate composite," *Rev. Sci. Instrum.*, vol. 83, no. 11, Nov. 2012, Art. no. 115001, doi: 10.1063/1.4763570.

[149] G. Lou, X. Yu, and R. Ban, "A wide-range DC current sensing method based on disk-type magnetoelectric laminate composite and magnetic concentrator," *Sensors Actuators A Phys.*, vol. 280, pp. 535–542, Sep. 2018, doi: 10.1016/j.sna.2018.08.029.

[150] W. Wang, Y. Huang, X. Liu, and Y. Liang, "Surface acoustic wave acceleration sensor with high sensitivity incorporating ST-X quartz cantilever beam," *Smart Mater. Struct.*, vol. 24, no. 1, Dec. 2015, Art. no. 015015, doi: 10.1088/0964-1726/24/1/015015.

[151] J. Labrenz et al., "Frequency response of SAW delay line magnetic field/current sensor," *IEEE Sensors Lett.*, vol. 3, no. 10, Oct. 2019, Art. no. 1500404, doi: 10.1109/LSENS.2019.2943129.

[152] R. Stoney, D. Geraghty, and G. E. O'Donnell, "Characterization of differentially measured strain using passive wireless surface acoustic wave (SAW) strain sensors," *IEEE Sensors J.*, vol. 14, no. 3, pp. 722–728, Mar. 2014, doi: 10.1109/jsen.2013.2285722.

[153] R. Steindi, C. Hausleitner, H. Hauser, and W. Bulst, "Wireless magnetic field sensor employing SAW-transponder," in *Proc. IEEE 12th Int. Symp. Appl. Ferroelect.*, 2000, vol. 2, pp. 855–858.
[154] B. Li, O. Yassine, and J. Kosel, "A surface acoustic wave passive and wireless sensor for magnetic fields, temperature, and humidity," *IEEE Sensors J.*, vol. 15, no. 1, pp. 453–462, Jan. 2015, doi: 10.1109/jsen.2014.2335058.
[155] A. K. Ganguly, K. L. Davis, D. C. Webb, C. Vittoria, and D. W. Forester, "Magnetically tuned surface-acoustic-wave phase shifter," *Electron. Lett.*, vol. 11, no. 25-26, pp. 610–611, Dec. 1975, doi: 10.1049/el:19750465.
[156] Y. Hui, T. X. Nan, N. X. Sun, and M. Rinaldi, "MEMS resonant magnetic field sensor based on an AlN/FeGaB bilayer nano-plate resonator," in *Proc. IEEE 26th Int. Conf. Micro Electro Mech. Syst.*, 2013, pp. 721–724.
[157] M. Li et al., "Ultra-sensitive NEMS magnetoelectric sensor for picotesla DC magnetic field detection," *Appl. Phys. Lett.*, vol. 110, no. 14, Apr. 2017, Art. no. 143510, doi: 10.1063/1.4979694.
[158] V. Polewczyk et al., "Unipolar and bipolar high-magnetic-field sensors based on surface acoustic wave resonators," *Phys. Rev. Appl.*, vol. 8, no. 2, Aug. 2017, Art. no. 024001, doi: 10.1103/PhysRevApplied.8.024001.
[159] X. Liu et al., "Influence of the delta-E effect on a surface acoustic wave resonator," *Appl. Phys. Lett.*, vol. 114, no. 6, Feb. 2019, Art. no. 062903, doi: 10.1063/1.5054977.
[160] H. Mishra et al., "Intrinsic versus shape anisotropy in microstructured magnetostrictive thin films for magnetic surface acoustic wave sensors," *Smart Mater. Struct.*, vol. 28, no. 12, Nov. 2019, Art. no. 12LT01, doi: 10.1088/1361-665X/ab522d.
[161] Y. Jia and W. Wang, "The development of SAW current sensor based on the magnetostrictive effect," in *Proc. Symp. Piezoelectricity Acoust. Waves, Device Appl.*, 2015, pp. 390–393.
[162] W. Wang, Y. Jia, X. Liu, Y. Liang, X. Xue, and Z. Du, "Enhanced sensitivity of temperature-compensated SAW-based current sensor using the magnetostrictive effect," *Smart Mater. Struct.*, vol. 26, no. 2, Dec. 2017, Art. no. 025008, doi: 10.1088/1361-665X/aa5137.
[163] G. Y. Karapetyan, V. A. Kalinin, M. E. Kutepov, V. O. Kislitsin, and E. M. Kaidashev, "SAW current sensor with FeNi film," in *Physics and Mechanics of New Materials and Their Applications,* I. A. Parinov, S. H. Chang, Y. H. Kim, and N. A. Noda, Eds., Berlin, Germany: Springer, 2021, pp. 533–538.
[164] T. Liu, X. Chen, Z. Di, J. Zhang, X. Li, and J. Chen, "Tunable magneto-optical wavelength filter of long-period fiber grating with magnetic fluids," *Appl. Phys. Lett.*, vol. 91, no. 12, 2007, Art. no. 121116, doi: 10.1063/1.2787970.
[165] F. B. Ajaei, M. Sanaye-Pasand, M. Davarpanah, A. Rezaei-Zare, and R. Iravani, "Compensation of the current-transformer saturation effects for digital relays," *IEEE Trans. Power Del.*, vol. 26, no. 4, pp. 2531–2540, Oct. 2011, doi: 10.1109/TPWRD.2011.2161622.
[166] T. Han, T. Jiang, Y. Liao, E. Wang, J. Chen, and S. Yang, "Simulation investigation on anti-DC current transformer with double core," in *Proc. IEEE 4th Int. Elect. Energy Conf.*, 2021, pp. 1–5, doi: 10.1109/CIEEC50170.2021.9510822.
[167] Z. Liren, P. Yang, and Z. Li, "Design and simulation of DC current comparator demodulation circuit," in *Proc. IEEE 14th Int. Conf. Electron. Meas. Instruments*, 2019, pp. 18–23, doi: 10.1109/ICEMI46757.2019.9101824.
[168] N. Wang et al., "Self-oscillating fluxgate-based quasi-digital sensor for DC high-current measurement," *IEEE Trans. Instrum. Meas.*, vol. 64, no. 12, pp. 3555–3563, Dec. 2015, doi: 10.1109/TIM.2015.2444258.
[169] Z. Zhao et al., "Current sensor utilizing giant magneto-impedance effect in amorphous ribbon toroidal core and CMOS inverter multivibrator," *Sensors Actuators A: Phys.*, vol. 137, no. 1, pp. 64–67, 2007, doi: 10.1016/j.sna.2007.02.037.
[170] P. Ripka, "Electric current sensors: A review," *Meas. Sci. Technol.*, vol. 21, no. 11, 2010, Art. no. 112001, doi: 10.1088/0957-0233/21/11/112001.

HONGYU SUN received the B.S degree in electrical engineering from the Department of Renewable Energy, North China Electric Power University, Beijing, China, in 2015, and the master's degree in electrical engineering from the Department of Electrical and Electronic Engineering, North China Electric Power University, Beijing, China, in 2018, and the Ph.D. degree in electrical engineering from the Department of Electrical Engineering, Tsinghua University, Beijing, in 2022.

He is currently a Lecturer with the School of Physical Science and Engineering, Beijing Jiaotong University, Beijing. His research interests include nondestructive evaluation (unidirectional and oblique focusing methods in horizontal and vertical shear waves), acoustic metamaterials (underwater acoustic focusing composite lens), plasma physics (Trichel pulse characteristics under the influence of photoionization), and artificial intelligence (using physics-informed deep learning algorithm to achieve the defect identification and quantification of ultrasound and MFL).

SONGLING HUANG (Senior Member, IEEE) received the bachelor's degree in automatic control engineering from Southeast University, Nanjing, China, in 1991, and the Ph.D. degree in nuclear application technology from Tsinghua University, Beijing, China, in 2001.

He is currently a Professor with the Department of Electrical Engineering, Tsinghua University, and he is also the Director of the Institute of New Electrical Technology and the Leader of the electromagnetic testing and equipment performance safety assessment team. His research interests include high-resolution detection of oil and gas pipeline corrosion defects, stress concentration detection and evaluation, active defect detection, pulsed eddy current detection sensor, and pipeline defect quantification and safety assessment.

LISHA PENG received the bachelor's degree in electrical engineering from the College of Electrical Engineering, Wuhan University, Hubei, China, in 2014, and the Ph.D. degree in electrical engineering from the Department of Electrical Engineering, Tsinghua University, Beijing, China, in 2019.

From 2019 to 2019, she was a Visiting Student with the School of Engineering and Computing Sciences, Durham University, Durham, U.K. She is currently a Postdoc with the Department of Electrical Engineering, Tsinghua University. Her current research interests include magnetic flux leakage (MFL) testing, electromagnetic ultrasonic guided wave testing, and nondestructive testing signal processing and defect evaluation.

Dr. Peng was the recipient of the Beijing Outstanding Graduates and the First Prize of Hubei Technological Invention Award.